

# TRANSIC: Sim-to-Real Policy Transfer by Learning from Online Correction

**Yunfan Jiang<sup>1</sup>, Chen Wang<sup>1</sup>, Ruohan Zhang<sup>1,2</sup>, Jiajun Wu<sup>1,2</sup>, Li Fei-Fei<sup>1,2</sup>**

<sup>1</sup>Department of Computer Science <sup>2</sup>Institute for Human-Centered AI (HAI)  
Stanford University

**Abstract:** Learning in simulation and transferring the learned policy to the real world has the potential to enable generalist robots. The key challenge of this approach is to address simulation-to-reality (sim-to-real) gaps. Previous methods often require domain-specific knowledge *a priori*. We argue that a straightforward way to obtain such knowledge is by asking humans to observe and assist robot policy execution in the real world. The robots can then learn from humans to close various sim-to-real gaps. We propose TRANSIC, a data-driven approach to enable successful sim-to-real transfer based on a human-in-the-loop framework. TRANSIC allows humans to augment simulation policies to overcome various unmodeled sim-to-real gaps holistically through intervention and online correction. Residual policies can be learned from human corrections and integrated with simulation policies for autonomous execution. We show that our approach can achieve successful sim-to-real transfer in complex and contact-rich manipulation tasks such as furniture assembly. Through synergistic integration of policies learned in simulation and from humans, TRANSIC is effective as a holistic approach to addressing various, often coexisting sim-to-real gaps. It displays attractive properties such as scaling with human effort. Videos and code are available at [transic-robot.github.io](https://transic-robot.github.io).

**Keywords:** Sim-to-Real Transfer, Human-in-the-Loop, Robot Manipulation

## 1 Introduction

Learning in simulation is a potential approach to the realization of generalist robots capable of solving sophisticated decision-making tasks [1, 2]. Learning to solve these tasks requires a large amount of training data [3–5]. Providing unlimited training supervision [6] through state-of-the-art simulation [7–11] could alleviate the burden of collecting data in the real world with physical robots [12, 13]. Therefore, it is crucial to seamlessly transfer and deploy robot control policies acquired in simulation, usually through reinforcement learning (RL), to real-world hardware. Successful demonstrations of this simulation-to-reality (sim-to-real) approach have been shown in dexterous in-hand manipulation [14–18], quadruped locomotion [19–22], biped locomotion [23–28], and quadrotor flight [29, 30].

Nevertheless, replicating similar success in manipulation tasks with robotic arms remains surprisingly challenging, with only a few cases in simple non-prehensile manipulation (such as pulling, pushing, and pivoting objects) [31–34], industry assembly under restricted settings [35–39], drawer opening [40], and peg swinging [40]. The difficulty mainly stems from the unavoidable sim-to-real gaps [11, 41], including but not limited to perception gap [19, 42–44], embodiment mismatch [19, 45, 46], controller inaccuracy [47–49], and dynamics realism [50]. Traditionally, researchers tackle these sim-to-real gaps and the transferring problem through system identification [19, 31, 51, 52], domain randomization [14, 53–55], real-world adaptation [56, 57], and simulator augmentation [58–60]. Many of these approaches require explicit, domain-specific knowledge and expertise on tasks or simulators. Although for a particular simulation-reality pair, there may

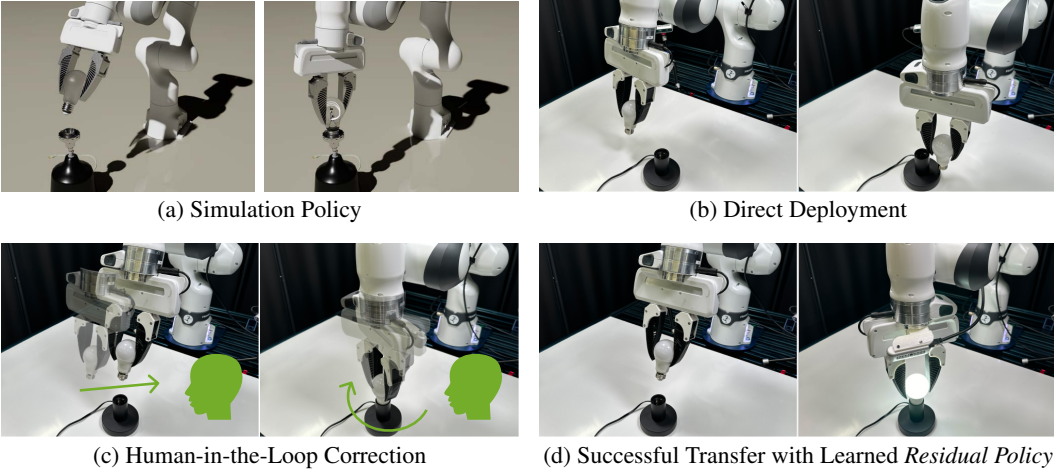


Figure 1: **TRANSIC for sim-to-real transfer in contact-rich robotic manipulation tasks.** **a)** and **b)** Naïvely deploying policies trained in simulation usually fails due to various sim-to-real gaps. Here, the robot attempts to first align the light bulb with the base and then insert and screw the light bulb into the base. **c)** A human operator monitors robot behaviors, intervenes, and provides online correction through teleoperation when necessary. Human data are collected to train a *residual policy* to tackle various sim-to-real gaps in a holistic manner. **d)** The simulation policy and residual policy are integrated together during test time to achieve successful sim-to-real transfer for contact-rich tasks, such as screwing a light bulb into the base.

exist specific inductive biases that can be hand-crafted *post hoc* to close the sim-to-real gap [19], such knowledge is often not available *a priori*. Identifying its effects on task completion is also intractable.

We argue that a straightforward and feasible way for humans to obtain such knowledge is to observe and assist policy execution in the real world. If humans can assist the robot to successfully accomplish the tasks in the real world, sim-to-real gaps are effectively addressed. This naturally leads to a generally applicable paradigm that can cover different priors across simulations and realities — human-in-the-loop learning [61–63] and shared-autonomy [64, 65].

Our key insight is that the human-in-the-loop framework is promising for addressing the sim-to-real gaps as a whole, in which humans directly assist the physical robots during policy execution by providing online correction signals. The knowledge required to close sim-to-real gaps can be learned from human signals. To this end, we present TRANSIC (**t**ransferring policies **s**im-to-**r**eal by **l**earning from **o**nline **c**orrection, Fig. 1), a data-driven approach to enable successful transferring of robot manipulation policies trained with RL in simulation to the real world. In TRANSIC, once the base robot policies are acquired from simulation training, they are deployed onto real robots where human operators monitor the execution. When the robot makes mistakes or gets stuck, humans interrupt and assist robot policies through teleoperation. Such human intervention data are collected to train a *residual policy*, after which the base policy and the residual policy are combined to solve contact-rich manipulation tasks, such as furniture assembly. With the synergistic integration with previous approaches, since humans can successfully assist the robot trained in silico to complete real-world tasks, sim-to-real gaps are implicitly handled and addressed by humans in a domain-agnostic manner. Additionally, human supervision naturally guarantees safe deployment.

To summarize, the key contribution of our work is a **novel, holistic human-in-the-loop method** called TRANSIC to tackle sim-to-real transfer of policies for manipulation tasks. Through extensive evaluation, we show that our method leads to **more effective sim-to-real transfer** compared to traditional methods [51, 53] and **requires less real-robot data** compared to the prevalent imitation learning and offline RL algorithms [66–69]. We demonstrate that successful sim-to-real transfer of short-horizon skills can solve **long-horizon, contact-rich manipulation** tasks in our daily activities, such as furniture assembly. Videos and code are available at [transic-robot.github.io](https://transic-robot.github.io).

## 2 Preliminaries

### 2.1 Problem Formulation

We formulate a robot manipulation task as an infinite-horizon discrete-time Partially Observable Markov Decision Process (POMDP)  $\mathcal{M} := (\mathcal{S}, \mathcal{O}, \Omega, \mathcal{A}, \mathcal{T}, R, \gamma, \rho_0)$ , where  $\mathcal{S}$  is the state space,  $\mathcal{O}$  is the observation space, and  $\mathcal{A}$  is the action space. At time step  $t$ , a robot observes  $o_t \in \mathcal{O}$  emitted from observation function  $\Omega(o_t|s_t, a_{t-1}) : \mathcal{S} \times \mathcal{A} \rightarrow \mathcal{O}$ , executes an action  $a_t$ , and receives a scalar reward  $r_t$  from the reward function  $R(s_t, a_t) : \mathcal{S} \times \mathcal{A} \rightarrow \mathbb{R}$ . The environment proceeds to the next state governed by the transition function  $\mathcal{T}(s_{t+1}|s_t, a_t) : \mathcal{S} \times \mathcal{A} \rightarrow \mathcal{S}$ . The robot learns a parameterized policy  $\pi_\theta(\cdot|o) : \mathcal{O} \rightarrow \Delta\mathcal{A}$  to maximize the expected discounted return  $\mathcal{J} := \mathbb{E}_{\tau \sim p_{\pi_\theta}} [\sum_{t=0}^{\infty} \gamma^t r_t]$  over induced trajectory distribution  $\tau := (s_0, o_0, a_0, r_0, \dots) \sim p_{\pi_\theta}$ , where  $s_0 \sim \rho_0$  is sampled from the initial state distribution. Additionally,  $\gamma \in [0, 1)$  is a discount factor. In this work, we model simulation and real environments as two different POMDPs.

### 2.2 Intervention-Based Policy Learning

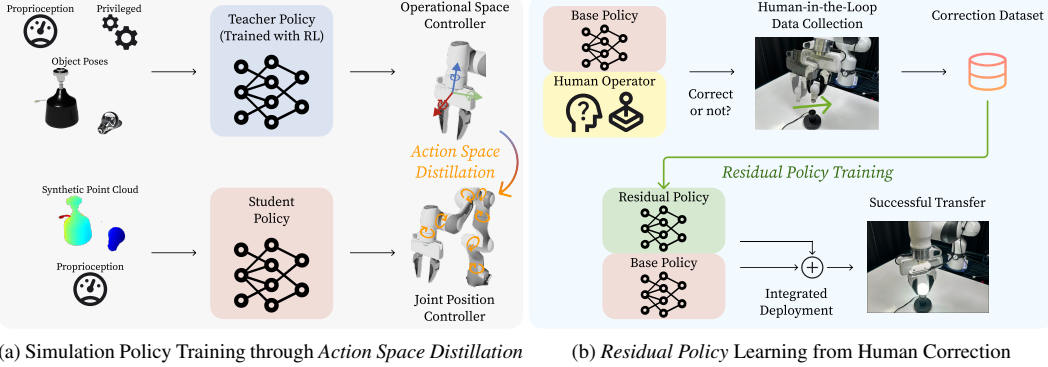
We adopt an intervention-based learning framework [66, 67, 70] where a human operator can intervene and take control during the execution of the robot base policy  $\pi_B$ . Denote the human policy as  $\pi_H$ , the following combined policy is deployed during data collection:  $\pi^{deployed} = \mathbf{1}^H \pi^H + (1 - \mathbf{1}^H) \pi^B$ , where  $\mathbf{1}^H$  is a binary function indicating human interventions. Introducing a trajectory distribution  $q(\tau)$  that consists of two observation-action distributions generated by the robot  $\rho^B$  and human operator  $\rho^H$ , the original RL objective leads to the maximization of a variational lower bound on logarithmic return [67, 71]:  $\mathcal{J}(\theta, q) = \mathbb{E}_{q(\tau)} [\log R(\tau) + \log p_{\pi_\theta} - \log q(\tau)]$ , where  $p_{\pi_\theta}$  is the induced trajectory distribution. While the human operator optimizes this objective through intervention and correction, the robot learner maximizes it through  $\theta = \arg \max_{\theta \in \Theta} \mathbb{E}_{(o, a) \sim q(\tau)} [\log \pi_\theta(a|o)]$ . Various intervention-based policy learning methods have been derived by weighting observation-action pairs differently. For example, HG-Dagger [66] completely ignores robot data  $\mathcal{D}^B$  and only trains on human data  $\mathcal{D}^H$  that contain intervention samples. This is equivalent to  $q(\tau) \propto \rho^H$ . Intervention Weighted Regression (IWR) [67] balances the data distribution by emphasizing human intervention:  $q(\tau) \propto \alpha \rho^H + \rho^B$  with  $\alpha = |\mathcal{D}^B|/|\mathcal{D}^H|$ . Non-intervention-based methods such as traditional behavior cloning (BC) [72] only learn on  $\mathcal{D}^H$  with full human demonstrations instead of intervention. This effectively sets  $q(\tau) \propto \rho^H$ .

## 3 TRANSIC: Sim-to-Real Policy Transfer by Learning from Online Correction

An overview of TRANSIC is shown in Fig. 2. At a high level, after training the base policy in simulation, we deploy it on the real robot while monitored by a human operator. The human interrupts the autonomous execution when necessary and provides online correction through teleoperation. Such intervention and online correction are collected to train a residual policy, after which both base and residual policies are deployed to complete contact-rich manipulation tasks. In this section, we first elaborate on the simulation training phase with several important design choices that reduce sim-to-real gaps before transfer. We then introduce residual policies learned from human intervention and online correction. Subsequently, we present an integrated framework for deploying the base policy alongside the learned residual policy during testing. Finally, we provide implementation details.

### 3.1 Learning Base Policies in Simulation with RL

**Policy Learning with 3D Representation** Object geometry matters for contact-rich manipulation. For example, a robot should ideally insert a light bulb into the lamp base with the thread facing down. To retain such 3D information and facilitate sim-to-real transfer, we propose to use point cloud as the main visual modality. Typical RGB observation used in visuomotor policy training [73] suffers from several drawbacks that hinder successful transfer, such as the vulnerability to different camera



(a) Simulation Policy Training through *Action Space Distillation*      (b) *Residual Policy* Learning from Human Correction

Figure 2: **TRANSIC method overview.** **a)** Base policies are first trained in simulation through *action space distillation* with demonstrations generated by RL teacher policies. Base policies take point cloud as input to reduce perception gap. **b)** After acquiring base policies, they are first deployed where a human operator monitors the execution. The human intervenes and corrects through teleoperation when necessary. Such intervention and correction data are collected to learn *residual policies*. Finally, both residual policies and base policies are integrated during test time to achieve successful transfer.

poses [74] and discrepancies between synthetic and real images [43]. Well-calibrated point cloud observation can bypass these issues and has been successfully demonstrated [15, 75]. During the simulation RL training phase, we synthesize point cloud observations for higher throughput. Concretely, given the synthetic point cloud of the  $m$ -th object  $\mathbf{P}^{(m)} \in \mathbb{R}^{K \times 3}$ , we transform it into the global frame through  $\mathbf{P}_g^{(m)} = \mathbf{P}^{(m)} (\mathbf{R}^{(m)})^\top + (\mathbf{p}^{(m)})^\top$ . Here  $\mathbf{R}^{(m)} \in \mathbb{R}^{3 \times 3}$  and  $\mathbf{p}^{(m)} \in \mathbb{R}^{3 \times 1}$  denote the object’s orientation and translation in the global frame. Further, the point cloud representation of a scene  $\mathbf{S}$  with  $M$  objects is aggregated as  $\mathbf{P}^{\mathbf{S}} = \bigcup_{m=1}^M \mathbf{P}_g^{(m)}$  and subsequently used as policy input.

**Action Space Distillation** A suitable action abstraction is critical for efficient learning [47, 48] as well as sim-to-real transfer [49]. A high-level controller such as the operational space controller (OSC) [76] facilitates RL exploration [47] but may hinder sim-to-real transfer because it requires accurate modeling of robot parameters, such as joint friction, mass, and inertia [77]; on the other hand, a low-level action space such as the joint position ensures consistent deployment in simulation and real hardware, but renders trial-and-error RL impractical. We draw inspiration from the teacher-student framework [16, 78–80] and propose to first train the teacher policy  $\pi^{teacher}$  through RL with OSC and then distill successful trajectories into the student policy  $\pi^{student}$  with joint position control. Specifically, we roll out  $\pi^{teacher}$  and record the robot’s joint position at every simulated time interval  $\delta t$  to construct a dataset  $\mathcal{D}^{teacher} = \{\tau^{(n)}\}_{n=1}^N$ . We then relabel actions from the end-effector’s poses to joint positions. Such a relabeled dataset is ready to train student policies through behavior cloning. We name this approach as *action space distillation* and find it crucial to overcome the sim-to-real controller gap. Furthermore, teacher policies directly receive privileged observations for ease of learning, while student policies learn on synthetic point-cloud inputs to match real-world measurements. The student policy parameterized by  $\theta$ ,  $\pi_\theta^{student}$ , is trained by minimizing the following loss function:

$$\mathcal{L}^{student} = -\mathbb{E}_{\mathcal{D}^{teacher}} [\log \pi_\theta^{student}] + \beta \mathbb{E}_{\mathcal{D}^{pcd}} [\|\phi(\mathbf{P}^{real}) - \phi(\mathbf{P}^{sim})\|^2], \quad (1)$$

where  $\phi(\cdot)$  denotes the point cloud encoder of  $\pi_\theta^{student}$  and  $\mathcal{D}^{pcd} = \{(\mathbf{P}^{real}, \mathbf{P}^{sim})^{(i)}\}_{i=1}^N$  is a separate dataset that contains  $N$  pairs of matched point clouds in simulation and reality for regularization purpose. We empirically justify the importance of such regularization in Sec. 4.5.

### 3.2 Learning Residual Policies from Online Correction

**Human-in-the-Loop Data Collection** Once the student policy is obtained from simulation, it is directly used as the base policy  $\pi^B$  to bootstrap the data collection. Naïvely deploying the base

policy on real robots usually results in inferior performance and unsafe motion due to various sim-to-real gaps. In TRANSIC, the base policy is instead deployed in a way that is fully synchronized with the human operator. Concretely, at time step  $t$ , once  $a_t^B \sim \pi^B$  is deployed, the execution is paused and a human operator needs to decide whether intervention is necessary, indicated as  $\mathbf{1}_t^H$ . Intervention is not necessary for most task execution when the robot is approaching objects of interest. However, when the robot tends to behave abnormally due to unaddressed sim-to-real gaps, the human operator intervenes and takes full control through teleoperation to correct robot errors. In these cases, the robot’s pre- and post-intervention states, as well as intervention indicator  $\mathbf{1}_t^H$ , are collected to construct the online correction dataset  $\mathcal{D}^H \leftarrow \mathcal{D}^H \cup (\mathbf{1}_t^H, \mathbf{q}_t^{pre}, \mathbf{q}_t^{post})$ . This procedure is illustrated in Algorithm 1.

**Human Correction as Residual Policies** Properly modeling human correction can be challenging. This is because humans usually solve tasks not purely based on current observation, hence the non-Markovian decision process [68]. Therefore, directly fine-tuning the base policy  $\pi^B$  on human correction dataset  $\mathcal{D}^H$  leads to large motions and even model collapse (Sec. 4). Inspired by prior work on learning residuals to compensate for unknown dynamics and noisy observations [81–83], we propose to incorporate human correction behaviors with *residual policies*. Concretely, at the time of intervention, a residual policy  $\pi_\psi^R$  parameterized by  $\psi$  learns to predict human intervention as the difference between post- and pre-intervention robot states:  $a^R = \mathbf{q}^{post} \ominus \mathbf{q}^{pre}$ , where  $\ominus$  denotes generalized subtraction. For continuous variables such as joint position, it computes the numerical difference; for binary variables such as opening and closing the gripper, it computes exclusive nor. The residual policy is then trained to maximize the likelihood of human correction:  $\mathcal{L}^{residual} = -\mathbb{E}_{\mathcal{D}^H} [\log \pi_\psi^R(a^R | \cdot)]$ .

### 3.3 An Integrated Deployment Framework

While in the original formulation of the residual policy, residual actions are always applied [82]. In practice, we find that learning a gating function to predict whether to apply the residual policy or not leads to smoother and more human-like behaviors. We call this *learned gated residual policy*. Denote the gating function as  $g_\psi(\cdot)$ . It can be trained through classification on  $\mathcal{D}^H$  and shares the same feature encoder with  $\pi^R$ . The policy effectively being deployed to autonomously complete tasks is an integration of base policy  $\pi^B$  and residual policy  $\pi^R$ , gated by  $g$ :  $\pi^{deployed} = \pi^B \oplus g\pi^R$ . A joint position controller is used during deployment.

### 3.4 Implementation Details

We use Isaac Gym [10] as the simulation backend. Proximal policy optimization (PPO [84]) is used to train teacher policies from scratch. We design task-specific reward functions and curricula when necessary to facilitate RL training. We apply exhaustive domain randomization during teacher policy training and proper data augmentation during student policy distillation. Student policies are parameterized as Gaussian Mixture Models (GMMs [68]). We have also experimented with other state-of-the-art policy models, such as Diffusion Policy [85], but did not observe better performances. See the Appendix Sec. A for more details about the simulation training phase and additional comparisons. During the human-in-the-loop data collection phase, we use a 3Dconnexion Space-Mouse as the teleoperation interface. Residual policies use state-of-the-art point cloud encoders, such as PointNet [86] and Perceiver [87, 88], and GMM as the action head. We follow the best practices to train residual policies, including using learning rate warm-up and cosine annealing [89]. More training hyperparameters are provided in the Appendix Sec. B.4.

## 4 Experiments

We seek to answer the following research questions with our experiments:

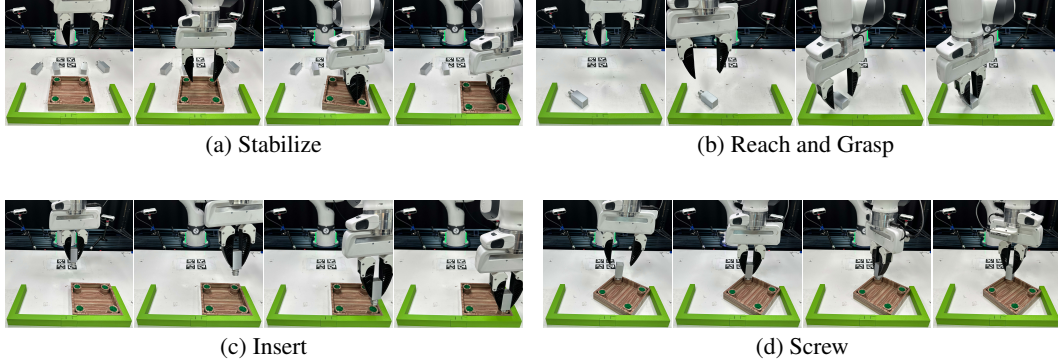


Figure 3: **Four tasks benchmarked in this work.** They are fundamental skills required to assemble a square table from FurnitureBench [90]. We randomize objects’ initial poses during evaluation. **a)** The robot pushes the square tabletop to the right corner of the wall such that it remains stable in following assembly steps. **b)** The robot reaches and grasps the table leg. It needs to properly adjust the end effector’s orientation to avoid infeasible grasping poses. **c)** The robot inserts the pre-grasped table leg to the far right assembly hole of the tabletop. **d)** The robot’s end-effector is initialized close to an inserted table leg and it screws the table leg clockwise into the tabletop.

- Q1:** Does TRANSIC lead to better transfer performance compared to traditional sim-to-real methods (Sec. 4.2)?
- Q2:** Can TRANSIC better integrate human correction into the policy learned in simulation than existing interactive imitation learning (IL) approaches (Sec. 4.2)?
- Q3:** Does TRANSIC require less real-world data to achieve good performance compared to algorithms that only learn from real-robot trajectories (Sec. 4.2)?
- Q4:** How effective can TRANSIC address different types of sim-to-real gaps (Sec. 4.3)?
- Q5:** How does TRANSIC scale with human effort (Sec. 4.4)?
- Q6:** Does TRANSIC exhibit intriguing properties, such as generalization to unseen objects, effective gating, policy robustness, consistency in learned visual features, ability to solve long-horizon manipulation tasks, and other emergent behaviors (Sec. 4.5)?

#### 4.1 Experiment Settings

**Tasks** We consider complex contact-rich manipulation tasks that require high precision in FurnitureBench [90]. These tasks are challenging and ideal for testing sim-to-real transfer, since perception, embodiment, controller, and dynamics gaps all need to be addressed to accomplish the tasks successfully. Specifically, we divide the assembly of a square table into four independent tasks (Fig. 3): *Stabilize*, *Reach and Grasp*, *Insert*, and *Screw*. We collect 20, 100, 90, and 17 real-robot trajectories with human correction, respectively. To further test the generalization to unseen objects from a new category, we experiment with a lamp (Fig. 6b). All experiments are conducted on a tabletop setting with a mounted Franka Emika 3 robot. See the Appendix Sec. B.1 for the detailed system setup.

**Baselines and Evaluation Protocol** We compare with the following three groups of baselines. **1) Traditional sim-to-real methods:** This group includes direct deployment of simulation policy trained with domain randomization and data augmentation [53], denoted as “DR. & Data Aug.”. It also covers the real-world fine-tuning paradigm, where simulation policies are further fine-tuned with real-robot data through BC (denoted as “BC Fine-Tune”) and the state-of-the-art offline RL method (implicit Q-learning [69], denoted as “IQL Fine-Tune”). To estimate the performance lower bound, we also include the baseline without any data augmentation or real-world fine-tuning, denoted as “Direct Transfer”. **2) Interactive IL:** This group represents the state-of-the-art interactive imitation learning methods, including HG-Dagger [66] and IWR [67]. **3) Learning from**

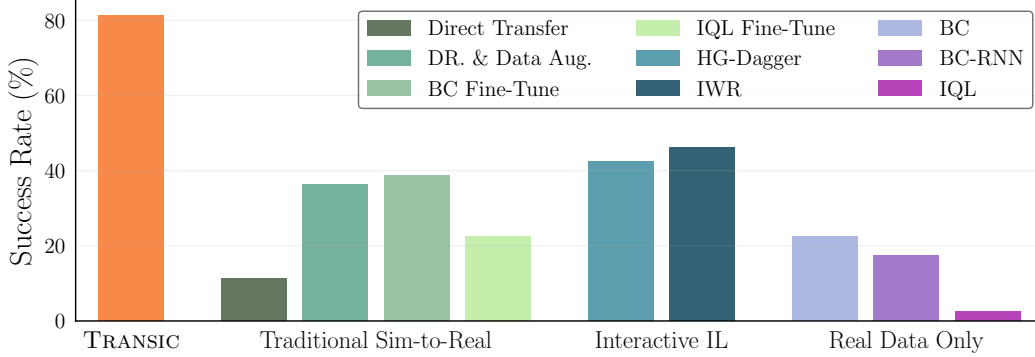


Figure 4: **Average success rates over four benchmarked tasks.** TRANSIC significantly outperforms three baseline groups. Results are success rates averaged over four tasks.

Table 1: **Success rates per tasks.** TRANSIC outperforms all baseline methods on all four tasks.

Tasks	TRANSIC	Direct Transfer	DR. & Data Aug. [53]	BC Fine-Tune	IQL Fine-Tune	HG-Dagger [66]	IWR [67]	BC [72]	BC-RNN [68]	IQL [69]
Stabilize	100%	10%	35%	55%	0%	65%	65%	40%	40%	5%
Reach and Grasp	95%	35%	60%	35%	0%	30%	40%	25%	0%	5%
Insert	45%	0%	15%	15%	25%	35%	40%	10%	5%	0%
Screw	85%	0%	35%	50%	65%	40%	40%	15%	25%	0%

**real-robot data only:** This group includes BC [72], BC-RNN [68], and IQL [69]. They are trained on real-robot demonstrations only. We follow Liu et al. [70] to label reward for IQL. All evaluations consist of 20 trials starting with different objects and robot poses. We make our best efforts to ensure the same initial settings when evaluating different methods. See Appendix Sec. C for the detailed evaluation protocol.

## 4.2 Quantitative Comparison on Four Assembly Tasks

As shown in Fig. 4 and Table 1, TRANSIC achieves the best performance on average and on all four tasks with significant margins. We now compare them in detail and discuss the main findings.

**TRANSIC is effective for sim-to-real transfer (Q1).** It successfully achieves a high average success rate of 81% across four tasks on real robots. For the task *Stabilize*, it can achieve a 100% success rate while the best baseline method (BC Fine-Tune) only succeeds half the time. For challenging tasks that require precise and contact-rich manipulation, such as *Insert* and *Screw*, TRANSIC results in promising outcomes (45% and 85% success rates, respectively) while the Direct Transfer baseline never succeeds.

What are the reasons for successful transfer? We observe that adding real-world human correction data does not guarantee improvement. For example, among traditional sim-to-real methods, the best baseline BC Fine-Tune outperforms DR. & Data Aug. by 7% but IQL Fine-Tune leads to worse performance. In contrast, TRANSIC effectively uses human correction data, which boosts average performance by 124%. Presumably, BC Fine-Tune’s marginal improvement is due to the domain difference between simulation and reality. This significant distinction cannot be easily bridged through naïve fine-tuning. Overall, TRANSIC not only achieves the best transfer performance, but also improves simulation policies the most among various sim-to-real approaches.

**TRANSIC can better incorporate human correction into the original learned policy (Q2).** Due to the differences between human and robot behaviors [68], using real-world data to directly fine-tune a policy that has been largely trained on machine-generated trajectories can lead to undesired performance. Specifically, TRANSIC outperforms interactive IL methods including HG-Dagger [66] and IWR [67] by 75% on average. While both of them weigh the intervention data higher during training (Sec. 2.2), we find that they tend to *erase* the original policy and lead to catastrophic forget-

ting. Therefore, in state space where no human intervention exists, they behave suboptimally and hence suffer from out-of-distribution issues due to compounding error. In contrast, by incorporating human correction with a separate residual policy and integrating both base and residual policies through gating, TRANSIC combines the best properties of both policies during deployment. It relies on the simulation policy for robust execution most of the time; when the base policy is likely to fail, it automatically applies the residual policy to prevent failures and correct mistakes.

### TRANSIC requires significantly less

**real-world data (Q3).** It only requires dozens of real-robot trajectories to achieve superior performance. However, methods such as BC-RNN and IQL trained on such a limited number of data suffer from overfitting and model collapse. TRANSIC achieves  $3.6\times$  better performance than them. In fact, as task complexity increases, we may need exponentially more real-world data to train these models, which solely rely on real-world demonstration data, according to the previous literature [68]. This result highlights the importance of training in simulation first, and then leveraging sim-to-real transfer for robot learning practitioners.

**Summary** we show that in sim-to-real transfer, a good base policy learned from the simulation can be combined with limited real-world data to achieve success (Q3). However, effectively utilizing human correction data to address the sim-to-real gap is challenging (Q1), especially when we want to prevent catastrophic forgetting of the base policy (Q2).

### 4.3 Effectiveness in Addressing Different Sim-to-Real Gaps (Q4)

While TRANSIC is a holistic approach to address multiple sim-to-real gaps simultaneously, we shed light on its ability to close each individual gap. To do so, we create five different simulation-reality pairs. For each of them, we intentionally create large gaps between the simulation and the real world. These gaps are applied to the real-world setting and they include *perception error*, *underactuated controller*, *embodiment mismatch*, *dynamics difference*, and *object asset mismatch*. Note that these are *artificial* settings for a controlled study. See the Appendix Sec. C.2 for detailed setups.

As shown in Fig. 5, TRANSIC achieves an average success rate of 77% across five different simulation-reality pairs with deliberately exacerbated sim-to-real gaps. This indicates its remarkable ability to close these individual gaps. In contrast, the best baseline method, IWR, only achieves an average success rate of 18%. We attribute this effectiveness in addressing different sim-to-real gaps to the residual policy design. Zeng et al. [83] echos our finding that residual learning is an effective tool to compensate for domain factors that cannot be explicitly modeled. Furthermore, training with data specifically collected from a particular setting generally increases TRANSIC’s performance. However, this is not the case for IWR, where fine-tuning on new data can even lead to worse performance. These results show that TRANSIC is better not only in addressing multiple sim-to-real gaps as a whole, but also in handling individual types of gaps of very different nature.

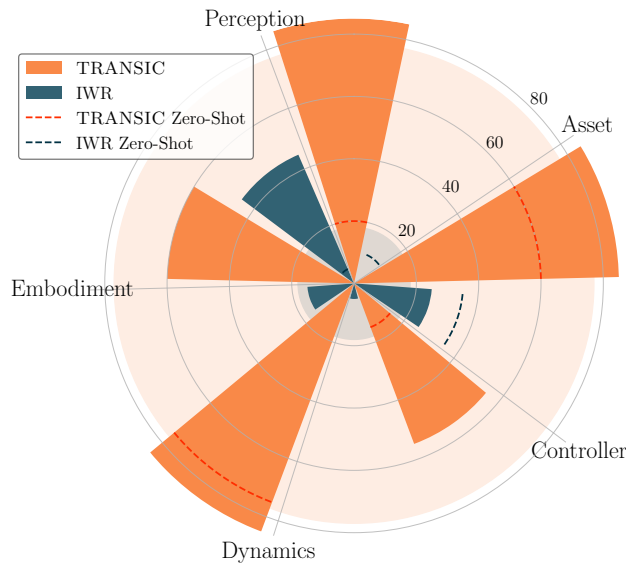


Figure 5: **Robustness to different sim-to-real gaps.** Numbers are averaged success rates (%). Polar bars represent performances after training with data collected specifically to address a particular gap. Dashed lines are zero-shot performances. Shaded circles show average performances.

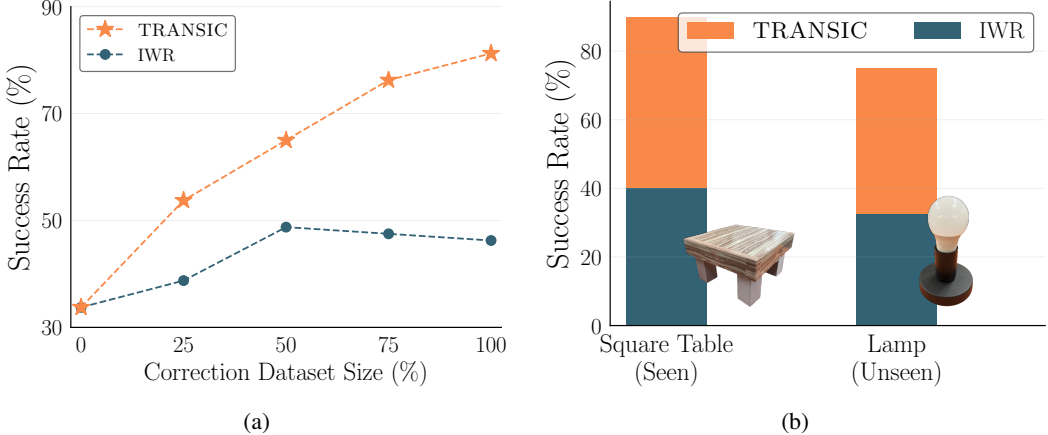


Figure 6: **a) Scalability with human correction data.** Numbers are success rates averaged over four tasks with different amount of human correction data. Per-task results are shown in Table A.XI. **b) Generalization to unseen objects from a new category.** Success rates are averaged over tasks *Reach* and *Grasp* and *Screw*.

#### 4.4 Scalability with Human Effort ( $\mathcal{Q}5$ )

Scaling with human effort is a desired property for human-in-the-loop robot learning methods [70]. We show that TRANSIC has better human data scalability than the best baseline IWR in Fig. 6a and Table A.XI. If we increase the size of the correction dataset from 25% to 75% of the full dataset size, TRANSIC achieves a relative improvement of 42% in the average success rate. In contrast, IWR only achieves 23% relative improvement. Additionally, for tasks other than *Insert*, IWR performance plateaus at an early stage and even starts to decrease as more human data becomes available. We hypothesize that IWR suffers from catastrophic forgetting and struggles to properly model the behavioral modes of humans and trained robots. On the other hand, TRANSIC bypasses these issues by learning gated residual policies only from human correction.

#### 4.5 Intriguing Properties and Emergent Behaviors ( $\mathcal{Q}6$ )

Finally, we examine further TRANSIC and discuss several emergent capabilities.

**Generalization to Unseen Objects** We show that a robot trained with TRANSIC can zero-shot generalize to new objects from a novel category. As shown in Fig. 6b, TRANSIC can achieve an average success rate of 75% when zero-shot evaluated on assembling a lamp. However, IWR can only succeed once every three attempts. This evidence suggests that TRANSIC is not overfitted to a particular object, instead, it has learned reusable skills for category-level object generalization.

**Effects of Different Gating Mechanisms** We introduce the learned gated residual policy in Sec. 3.3 where the gating mechanism controls when to apply residual actions. To assess the quality of learned gating, we compare its performance with an actual human operator performing gating. Results are shown in Table 2. It is evident that the learned gating mechanism only incurs negligible performance drops compared to human gating. This suggests that TRANSIC can reliably operate in a fully autonomous setting once the gating mechanism is learned.

**Policy Robustness** We investigate the policy robustness against 1) point cloud observations with inferior quality by removing two cameras, and 2) suboptimal correction data with noise injection. See Appendix Sec. C.4 for detailed experiment setups. Results are shown in Table 2. We highlight that TRANSIC is robust to partial point cloud inputs caused by the reduced number of cameras. We attribute this to the heavy point cloud downsampling employed during training. Fishman et al. [91] echos our finding that policies trained with downsampled synthetic point cloud inputs can

Table 2: **Results of ablation studies.** We study the effects of different gating mechanisms (learned gating vs human gating), policy robustness against reduced cameras and suboptimal correction data, and the importance of visual encoder regularization.

	Average	Stabilize	Reach and Grasp	Insert	Screw
Original	81%	100%	95%	45%	85%
w/ Human Gating	82%	100%	95%	50%	85%
Reduced Cameras	80%	95%	90%	40%	95%
Noisy Correction	76%	85%	80%	45%	95%
w/o Regularization	55%	85%	55%	20%	60%

generalize to partial point cloud observations obtained in the real world without the need for shape completion. Meanwhile, when the correction data used to learn residual policies are suboptimal, TRANSIC only shows a relative decrease of 6% in the average success rate. We attribute this to the advantage of our integrated deployment — when the residual policy behaves suboptimally, the base policy could still compensate for the error in subsequent steps.

**Importance of Point Cloud Encoder Regularization** To learn consistent visual features between the simulation and reality, we propose to regularize the point cloud encoder during the distillation stage as in Eq. 1. As shown in Table 2, the performance significantly decreases without such regularization, especially for tasks that require fine-grained visual features. Without it, simulation policies would overfit to synthetic point cloud observations and hence are not ideal for sim-to-real transfer.

**Qualitative Analysis and Emergent Behaviors** We first examine the distribution of the collected human correction dataset. During the human-in-the-loop data collection, the probability of intervening and correcting is reasonably low ( $P_{\text{correction}} \approx 0.20$ ). This is consistent with our intuition that, with a good base policy, interventions are not necessary for most of the time. However, they become critical when the robot tends to behave abnormally due to unaddressed sim-to-real gaps. Moreover, as highlighted in Fig. A.8, interventions happen at different times across tasks. This fact renders heuristics-based methods [92] for deciding when to intervene difficult, and further necessitates our learned residual policy.

Surprisingly, TRANSIC shows several representative behaviors that resemble humans. For instance, they include error recovery, unsticking, safety-aware actions, and failure prevention as shown in Fig. 7.

**Solving Long-Horizon Manipulation Tasks** Finally, we demonstrate that successful sim-to-real transfer of individual skills can be effectively chained together to enable long-horizon contact-rich manipulation (Fig. 8). See videos on [transic-robot.github.io](https://transic-robot.github.io) for a robot assembling a square table and a lamp using TRANSIC.

## 5 Related Work

**Robot Learning via Sim-to-Real Transfer** Physics-based simulations [7–11, 50, 93–95] have become a driving force [1, 2] for developing robotic skills in tabletop manipulation [96–99], mobile manipulation [100–103], fluid and deformable object manipulation [104–107], dexterous in-hand manipulation [14–18], locomotion with various robot morphology [19–27, 108], object tossing [83], acrobatic flight [29, 30], etc. However, the domain gap between the simulators and the reality is not negligible [11]. Successful sim-to-real transfer includes locomotion [19–28], in-hand re-orientation for dexterous hands where objects are initially placed near the robot [14–18], and non-prehensile manipulation limited to simple tasks [31–40]. In this work, we tackle more challenging sim-to-real transfer for complex manipulation tasks and successfully demonstrate that our approach can solve sophisticated contact-rich manipulation tasks. More importantly, it requires significantly fewer real-

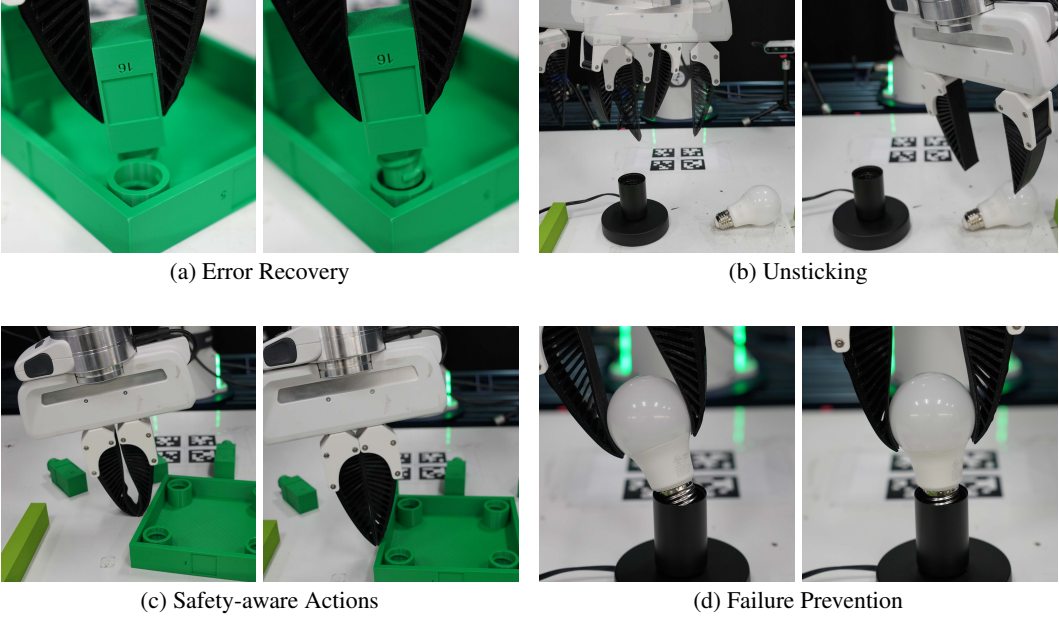
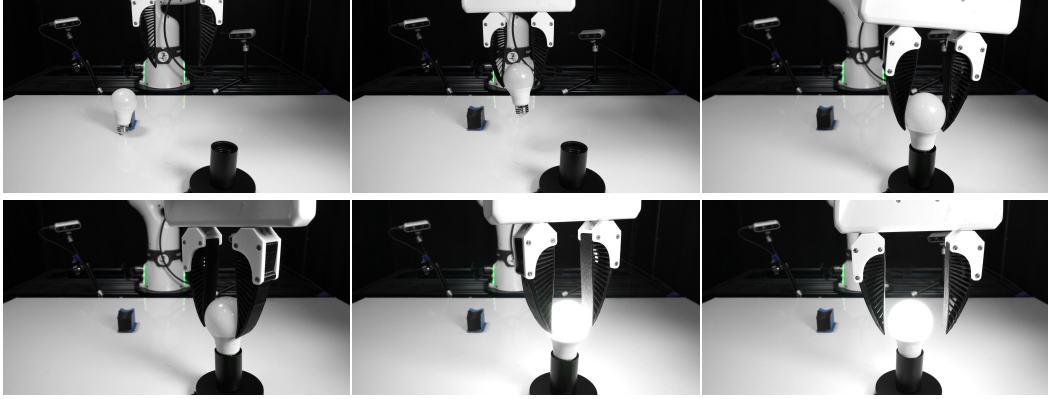


Figure 7: **Emergent behaviors learned by TRANSIC.** **a) Error recovery.** Left: The robot tries to insert the table leg but the direction is wrong; Right: TRANSIC raises the end effector and moves to the correct insertion position. **b) Unsticking.** Left: The robot hovers for a while and never reaches the light bulb; Right: TRANSIC helps the robot get unstuck and move to the bulb. **c) Safety-aware actions.** Left: When pushing the tabletop, the gripper is too low and bends. This might damage the robot; Right: TRANSIC compensates for the command that causes the end effector to move too low. **d) Failure prevention.** Left: The light bulb will fall and break after gripper opening; Right: TRANSIC adjusts the bulb to a stable pose to prevent failure.

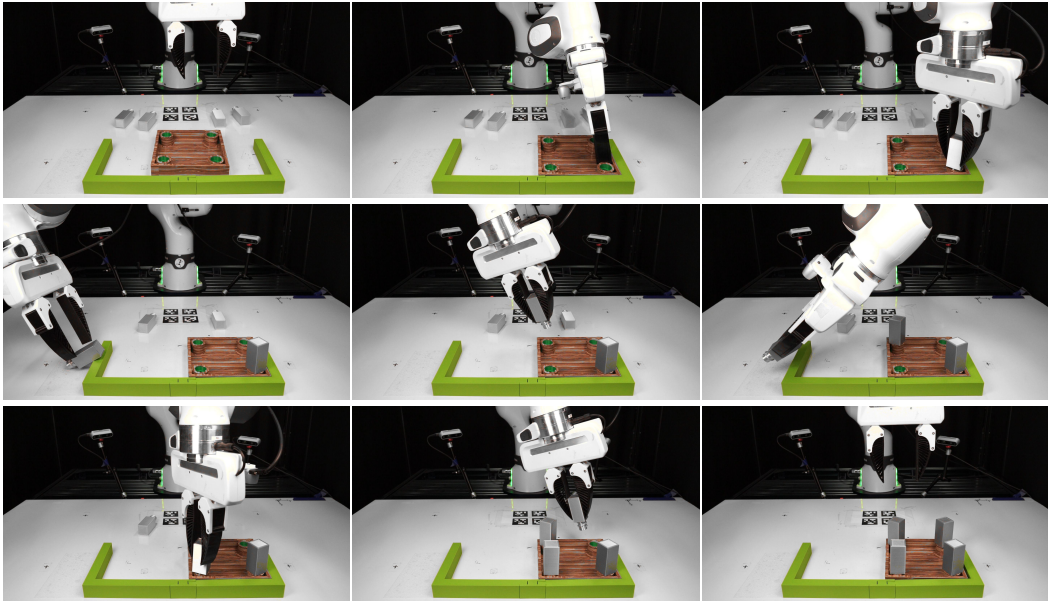
robot data compared to the prevalent imitation learning and offline RL approaches [68, 69, 72]. This makes solutions that are based on simulators and sim-to-real transfer more appealing to roboticists.

**Sim-to-Real Gaps in Manipulation Tasks** Despite the complex manipulation skills recently learned with RL in simulation [109], directly deploying learned control policies to physical robots often fails. The sim-to-real gaps [11, 41, 45, 110] that contribute to this performance discrepancy can be coarsely categorized as follows: **a)** perception gap [19, 42–44], where synthetic sensory observations differ from those measured in the real world; **b)** embodiment mismatch [19, 45, 46], where the robot models used in simulation do not match the real-world hardware precisely; **c)** controller inaccuracy [47–49], meaning that the results of deploying the same high-level commands (such as in configuration space [111] and task space [112]) differ in simulation and real hardware; and **d)** poor physical realism [50], where physical interactions such as contact and collision are poorly simulated [113].

Although these gaps may not be fully bridged, traditional methods to address them include system identification [19, 31, 51, 52], domain randomization [14, 53–55], real-world adaptation [56], and simulator augmentation [58–60]. However, system identification is mostly engineered on a case-by-case basis. Domain randomization suffers from the inability to identify and randomize all physical parameters. Methods with real-world adaptation, usually through meta-learning [114], incur potential safety concerns during the adaptation phase. Most of these approaches also rely on explicit and domain-specific knowledge about tasks and the simulator *a priori*. For instance, to perform system identification for closing the embodiment gap for a quadruped, Tan et al. [19] disassembles the physical robot and carefully calibrates parameters including size, mass, and inertia. Kim et al. [33] reports that collaborative robots, such as the commonly used Franka Emika robot, have intricate joint friction that is hard to identify and randomized in typical physics simulators. To make a simulator more akin to the real world, Chebotar et al. [40] deploys trained virtual robots multi-



(a) Assemble a lamp.



(b) Assemble a square table.

Figure 8: We demonstrate that individual skills learned with TRANSIC can be effectively chained together to enable long-horizon contact-rich manipulation. a) The robot assembles a lamp (160 seconds in 1× speed). b) The robot assembles a square table from FurnitureBench [90] (550 seconds in 1× speed). Videos are available on [transic-robot.github.io](https://transic-robot.github.io).

ple times to refine the distributions of simulation parameters. This procedure not only introduces a significant real-world sampling effort, but also incurs potential safety concerns due to deploying sub-optimal policies. In contrast, our method leverages human intervention data to implicitly overcome the transferring problem in a domain-agnostic way and also leads to safer deployment.

**Human-in-The-Loop Robot Learning** Human-in-the-loop machine learning is a prevalent framework to inject human knowledge into autonomous systems [62, 115, 116]. Various forms of human feedback exist [63], ranging from passive judgement, such as preference [117–126] and evaluation [127–132], to active involvement, including intervention [133–135] and correction [136, 137]. They are widely adopted in solutions for sequential decision-making tasks. For instance, interactive imitation learning [66, 67, 70, 138] leverages human intervention and correction to help naïve imitators address data mismatch and compounding error. In the context of RL, reward functions can be derived to better align agent behaviors with human preferences [120, 123, 124, 127]. Noticeably,

recent trend focuses on continually improving robots’ capability by iteratively updating and deploying policies with human feedback [70], combining active human involvement with RL [137], and autonomously generating corrective intervention data [139]. Our work further extends this trend by showing that sim-to-real gaps can be effectively eliminated by using human intervention and correction signals.

In shared autonomy, robots and humans share the control authority to achieve a common goal [64, 65, 140–142]. This control paradigm has been largely studied in assistive robotics and human-robot collaboration [143–145]. In this work, we provide a novel perspective by employing it in sim-to-real transfer of robot control policies and demonstrating its importance in attaining effective transfer.

## 6 Conclusion and Limitations

In this work, we present TRANSIC, a holistic human-in-the-loop method to tackle sim-to-real transfer of policies for contact-rich manipulation tasks. We show that in sim-to-real transfer, a good base policy learned from the simulation can be combined with limited real-world data to achieve success. However, effectively utilizing human correction data to address the sim-to-real gap is challenging, especially when we want to prevent catastrophic forgetting of the base policy. TRANSIC successfully addresses these challenges by learning a gated residual policy from human correction data. We show that TRANSIC is effective as a holistic approach to address different types of sim-to-real gaps when presented simultaneously; it is also effective as an approach to address individual gaps of very different natures. It displays attractive properties, such as scaling with human effort.

While TRANSIC achieves remarkable sim-to-real transfer results, it still has several limitations which should be addressed by follow-up studies. 1) The current tasks are limited to the tabletop scenario with a soft parallel-jaw gripper. However, we notice that with the development of teleoperation devices for more complicated robots, such as bimanual arms [146], dexterous hands [147], mobile manipulators [148, 149], and humanoids [150], TRANSIC can also be potentially applied to these settings. 2) During the correction data collection phase, the human operator still manually decides when to intervene. This effort might be reduced by leveraging automatic failure detection techniques [151, 152]. 3) TRANSIC requires simulation policies with reasonable performances in the first place, which is challenging to learn by itself. Nevertheless, TRANSIC is compatible with and can benefit from recent advances in this direction [6, 85, 153].

## Acknowledgments

We are grateful to Josiah Wong, Chengshu (Eric) Li, Weiyu Liu, Wenlong Huang, Stephen Tian, Sanjana Srivastava, and the SVL PAIR group for their helpful feedback and insightful discussions. This work is in part supported by the Stanford Institute for Human-Centered AI (HAI), ONR MURI N00014-22-1-2740, ONR MURI N00014-21-1-2801, and Schmidt Sciences. Ruohan Zhang is partially supported by Wu Tsai Human Performance Alliance Fellowship.

## References

- [1] H. Choi, C. Crump, C. Duriez, A. Elmquist, G. Hager, D. Han, F. Hearl, J. Hodgins, A. Jain, F. Leve, C. Li, F. Meier, D. Negru, L. Righetti, A. Rodriguez, J. Tan, and J. Trinkle. On the use of simulation in robotics: Opportunities, challenges, and suggestions for moving forward. *Proceedings of the National Academy of Sciences*, 118(1):e1907856118, 2021. doi:10.1073/pnas.1907856118. URL <https://www.pnas.org/doi/abs/10.1073/pnas.1907856118>.
- [2] C. K. Liu and D. Negru. The role of physics-based simulators in robotics. *Annual Review of Control, Robotics, and Autonomous Systems*, 4(1):35–58, 2021. doi:10.1146/annurev-control-072220-093055. URL <https://doi.org/10.1146/annurev-control-072220-093055>.
- [3] P. Abbeel and A. Y. Ng. Apprenticeship learning via inverse reinforcement learning. In *Proceedings of the Twenty-First International Conference on Machine Learning*, ICML ’04, page 1, New York, NY, USA, 2004. Association for Computing Machinery. ISBN 1581138385. doi:10.1145/1015330.1015430. URL <https://doi.org/10.1145/1015330.1015430>.
- [4] H. D. III, J. Langford, and D. Marcu. Search-based structured prediction. *arXiv preprint arXiv: Arxiv-0907.0786*, 2009.
- [5] S. Yang, O. Nachum, Y. Du, J. Wei, P. Abbeel, and D. Schuurmans. Foundation models for decision making: Problems, methods, and opportunities. *arXiv preprint arXiv: Arxiv-2303.04129*, 2023.
- [6] A. Mandlekar, S. Nasiriany, B. Wen, I. Akinola, Y. Narang, L. Fan, Y. Zhu, and D. Fox. Mimicgen: A data generation system for scalable robot learning using human demonstrations. *arXiv preprint arXiv: Arxiv-2310.17596*, 2023.
- [7] E. Todorov, T. Erez, and Y. Tassa. Mujoco: A physics engine for model-based control. *2012 IEEE/RSJ International Conference on Intelligent Robots and Systems*, pages 5026–5033, 2012. doi:10.1109/IROS.2012.6386109.
- [8] E. Coumans and Y. Bai. Pybullet, a python module for physics simulation for games, robotics and machine learning. <http://pybullet.org>, 2016–2021.
- [9] Y. Zhu, J. Wong, A. Mandlekar, R. Martín-Martín, A. Joshi, S. Nasiriany, and Y. Zhu. robosuite: A modular simulation framework and benchmark for robot learning. *arXiv preprint arXiv: Arxiv-2009.12293*, 2020.
- [10] V. Makoviychuk, L. Wawrzyniak, Y. Guo, M. Lu, K. Storey, M. Macklin, D. Hoeller, N. Rudin, A. Allshire, A. Handa, and G. State. Isaac gym: High performance gpu-based physics simulation for robot learning. *arXiv preprint arXiv: Arxiv-2108.10470*, 2021.
- [11] C. Li, C. Gokmen, G. Levine, R. Martín-Martín, S. Srivastava, C. Wang, J. Wong, R. Zhang, M. Lingelbach, J. Sun, M. Anvari, M. Hwang, M. Sharma, A. Aydin, D. Bansal, S. Hunter, K.-Y. Kim, A. Lou, C. R. Matthews, I. Villa-Renteria, J. H. Tang, C. Tang, F. Xia, S. Savarese, H. Gweon, K. Liu, J. Wu, and L. Fei-Fei. BEHAVIOR-1k: A benchmark for embodied AI with 1,000 everyday activities and realistic simulation. In *6th Annual Conference on Robot Learning*, 2022. URL [https://openreview.net/forum?id=\\_8DoIe8G3t](https://openreview.net/forum?id=_8DoIe8G3t).
- [12] A. Brohan, N. Brown, J. Carbajal, Y. Chebotar, J. Dabis, C. Finn, K. Gopalakrishnan, K. Hausman, A. Herzog, J. Hsu, J. Ibarz, B. Ichter, A. Irpan, T. Jackson, S. Jesmonth, N. J. Joshi, R. Julian, D. Kalashnikov, Y. Kuang, I. Leal, K.-H. Lee, S. Levine, Y. Lu, U. Malla, D. Manjunath, I. Mordatch, O. Nachum, C. Parada, J. Peralta, E. Perez, K. Pertsch, J. Quiambao, K. Rao, M. Ryoo, G. Salazar, P. Sanketi, K. Sayed, J. Singh, S. Sontakke,

- A. Stone, C. Tan, H. Tran, V. Vanhoucke, S. Vega, Q. Vuong, F. Xia, T. Xiao, P. Xu, S. Xu, T. Yu, and B. Zitkovich. Rt-1: Robotics transformer for real-world control at scale. *arXiv preprint arXiv: Arxiv-2212.06817*, 2022.
- [13] K. Bousmalis, G. Vezzani, D. Rao, C. Devin, A. X. Lee, M. Bauza, T. Davchev, Y. Zhou, A. Gupta, A. Raju, A. Laurens, C. Fantacci, V. Dalibard, M. Zambelli, M. Martins, R. Pevcovic, M. Blokzijl, M. Denil, N. Batchelor, T. Lampe, E. Parisotto, K. Źołna, S. Reed, S. G. Colmenarejo, J. Scholz, A. Abdolmaleki, O. Groth, J.-B. Regli, O. Sushkov, T. Rothörl, J. E. Chen, Y. Aytar, D. Barker, J. Ortiz, M. Riedmiller, J. T. Springenberg, R. Hadsell, F. Nori, and N. Heess. Robocat: A self-improving generalist agent for robotic manipulation. *arXiv preprint arXiv: Arxiv-2306.11706*, 2023.
  - [14] OpenAI, I. Akkaya, M. Andrychowicz, M. Chociej, M. Litwin, B. McGrew, A. Petron, A. Paino, M. Plappert, G. Powell, R. Ribas, J. Schneider, N. Tezak, J. Tworek, P. Welinder, L. Weng, Q. Yuan, W. Zaremba, and L. Zhang. Solving rubik’s cube with a robot hand. *arXiv preprint arXiv: Arxiv-1910.07113*, 2019.
  - [15] T. Chen, M. Tippur, S. Wu, V. Kumar, E. Adelson, and P. Agrawal. Visual dexterity: In-hand reorientation of novel and complex object shapes. *Science Robotics*, 8(84):eadc9244, 2023. doi:10.1126/scirobotics.adc9244. URL <https://www.science.org/doi/abs/10.1126/scirobotics.adc9244>.
  - [16] Y. Chen, C. Wang, L. Fei-Fei, and C. K. Liu. Sequential dexterity: Chaining dexterous policies for long-horizon manipulation. *arXiv preprint arXiv: Arxiv-2309.00987*, 2023.
  - [17] H. Qi, A. Kumar, R. Calandra, Y. Ma, and J. Malik. In-hand object rotation via rapid motor adaptation. *arXiv preprint arXiv: Arxiv-2210.04887*, 2022.
  - [18] H. Qi, B. Yi, S. Suresh, M. Lambeta, Y. Ma, R. Calandra, and J. Malik. General in-hand object rotation with vision and touch. *arXiv preprint arXiv: Arxiv-2309.09979*, 2023.
  - [19] J. Tan, T. Zhang, E. Coumans, A. Iscen, Y. Bai, D. Hafner, S. Bohez, and V. Vanhoucke. Sim-to-real: Learning agile locomotion for quadruped robots. *arXiv preprint arXiv: Arxiv-1804.10332*, 2018.
  - [20] A. Kumar, Z. Fu, D. Pathak, and J. Malik. RMA: rapid motor adaptation for legged robots. In D. A. Shell, M. Toussaint, and M. A. Hsieh, editors, *Robotics: Science and Systems XVII, Virtual Event, July 12-16, 2021*, 2021. doi:10.15607/RSS.2021.XVII.011. URL <https://doi.org/10.15607/RSS.2021.XVII.011>.
  - [21] Z. Zhuang, Z. Fu, J. Wang, C. Atkeson, S. Schwertfeger, C. Finn, and H. Zhao. Robot parkour learning. *arXiv preprint arXiv: Arxiv-2309.05665*, 2023.
  - [22] R. Yang, G. Yang, and X. Wang. Neural volumetric memory for visual locomotion control. *arXiv preprint arXiv: Arxiv-2304.01201*, 2023.
  - [23] H. Benbrahim and J. A. Franklin. Biped dynamic walking using reinforcement learning. *Robotics and Autonomous Systems*, 22(3):283–302, 1997. ISSN 0921-8890. doi: [https://doi.org/10.1016/S0921-8890\(97\)00043-2](https://doi.org/10.1016/S0921-8890(97)00043-2). URL <https://www.sciencedirect.com/science/article/pii/S0921889097000432>. Robot Learning: The New Wave.
  - [24] G. A. Castillo, B. Weng, W. Zhang, and A. Hereid. Reinforcement learning-based cascade motion policy design for robust 3d bipedal locomotion. *IEEE Access*, 10:20135–20148, 2022. doi:10.1109/ACCESS.2022.3151771.
  - [25] L. Krishna, G. A. Castillo, U. A. Mishra, A. Hereid, and S. Kolathaya. Linear policies are sufficient to realize robust bipedal walking on challenging terrains. *arXiv preprint arXiv: Arxiv-2109.12665*, 2021.

- [26] J. Siekmann, K. Green, J. Warila, A. Fern, and J. Hurst. Blind bipedal stair traversal via sim-to-real reinforcement learning. *arXiv preprint arXiv: Arxiv-2105.08328*, 2021.
- [27] I. Radosavovic, T. Xiao, B. Zhang, T. Darrell, J. Malik, and K. Sreenath. Real-world humanoid locomotion with reinforcement learning. *arXiv preprint arXiv: Arxiv-2303.03381*, 2023.
- [28] Z. Li, X. B. Peng, P. Abbeel, S. Levine, G. Berseth, and K. Sreenath. Reinforcement learning for versatile, dynamic, and robust bipedal locomotion control. *arXiv preprint arXiv: Arxiv-2401.16889*, 2024.
- [29] E. Kaufmann, L. Bauersfeld, A. Loquercio, M. Müller, V. Koltun, and D. Scaramuzza. Champion-level drone racing using deep reinforcement learning. *Nature*, 2023. doi:10.1038/s41586-023-06419-4. URL <https://doi.org/10.1038/s41586-023-06419-4>.
- [30] Y. Song, A. Romero, M. Müller, V. Koltun, and D. Scaramuzza. Reaching the limit in autonomous racing: Optimal control versus reinforcement learning. *Science Robotics*, 8(82):eadg1462, 2023. doi:10.1126/scirobotics.adg1462. URL <https://www.science.org/doi/abs/10.1126/scirobotics.adg1462>.
- [31] V. Lim, H. Huang, L. Y. Chen, J. Wang, J. Ichnowski, D. Seita, M. Laskey, and K. Goldberg. Planar robot casting with real2sim2real self-supervised learning. *arXiv preprint arXiv: Arxiv-2111.04814*, 2021.
- [32] W. Zhou and D. Held. Learning to grasp the ungraspable with emergent extrinsic dexterity. In K. Liu, D. Kulic, and J. Ichnowski, editors, *Conference on Robot Learning, CoRL 2022, 14-18 December 2022, Auckland, New Zealand*, volume 205 of *Proceedings of Machine Learning Research*, pages 150–160. PMLR, 2022. URL <https://proceedings.mlr.press/v205/zhou23a.html>.
- [33] M. Kim, J. Han, J. Kim, and B. Kim. Pre- and post-contact policy decomposition for non-prehensile manipulation with zero-shot sim-to-real transfer. *arXiv preprint arXiv: Arxiv-2309.02754*, 2023.
- [34] X. Zhang, S. Jain, B. Huang, M. Tomizuka, and D. Romeres. Learning generalizable pivoting skills. In *IEEE International Conference on Robotics and Automation, ICRA 2023, London, UK, May 29 - June 2, 2023*, pages 5865–5871. IEEE, 2023. doi:10.1109/ICRA48891.2023.10161271. URL <https://doi.org/10.1109/ICRA48891.2023.10161271>.
- [35] S. Kozlovsky, E. Newman, and M. Zackenhouse. Reinforcement learning of impedance policies for peg-in-hole tasks: Role of asymmetric matrices. *IEEE Robotics and Automation Letters*, 7(4):10898–10905, 2022. doi:10.1109/LRA.2022.3191070.
- [36] D. Son, H. Yang, and D. Lee. Sim-to-real transfer of bolting tasks with tight tolerance. In *2020 IEEE/RSJ International Conference on Intelligent Robots and Systems (IROS)*, pages 9056–9063, 2020. doi:10.1109/IROS45743.2020.9341644.
- [37] B. Tang, M. A. Lin, I. Akinola, A. Handa, G. S. Sukhatme, F. Ramos, D. Fox, and Y. S. Narang. Industreal: Transferring contact-rich assembly tasks from simulation to reality. In K. E. Bekris, K. Hauser, S. L. Herbert, and J. Yu, editors, *Robotics: Science and Systems XIX, Daegu, Republic of Korea, July 10-14, 2023*, 2023. doi:10.15607/RSS.2023.XIX.039. URL <https://doi.org/10.15607/RSS.2023.XIX.039>.
- [38] X. Zhang, C. Wang, L. Sun, Z. Wu, X. Zhu, and M. Tomizuka. Efficient sim-to-real transfer of contact-rich manipulation skills with online admittance residual learning. In *7th Annual Conference on Robot Learning*, 2023. URL <https://openreview.net/forum?id=gFXVysXh48K>.

- [39] X. Zhang, M. Tomizuka, and H. Li. Bridging the sim-to-real gap with dynamic compliance tuning for industrial insertion. *arXiv preprint arXiv: Arxiv-2311.07499*, 2023.
- [40] Y. Chebotar, A. Handa, V. Makoviychuk, M. Macklin, J. Issac, N. Ratliff, and D. Fox. Closing the sim-to-real loop: Adapting simulation randomization with real world experience. *arXiv preprint arXiv: Arxiv-1810.05687*, 2018.
- [41] N. Jakobi, P. Husbands, and I. Harvey. Noise and the reality gap: The use of simulation in evolutionary robotics. In F. Morán, A. Moreno, J. J. Merelo, and P. Chacón, editors, *Advances in Artificial Life*, pages 704–720, Berlin, Heidelberg, 1995. Springer Berlin Heidelberg. ISBN 978-3-540-49286-3.
- [42] E. Tzeng, C. Devin, J. Hoffman, C. Finn, X. Peng, S. Levine, K. Saenko, and T. Darrell. Towards adapting deep visuomotor representations from simulated to real environments. *ArXiv*, abs/1511.07111, 2015. URL <https://api.semanticscholar.org/CorpusID:1541419>.
- [43] K. Bousmalis, A. Irpan, P. Wohlhart, Y. Bai, M. Kelcey, M. Kalakrishnan, L. Downs, J. Ibarz, P. Pastor, K. Konolige, S. Levine, and V. Vanhoucke. Using simulation and domain adaptation to improve efficiency of deep robotic grasping. *arXiv preprint arXiv: Arxiv-1709.07857*, 2017.
- [44] D. Ho, K. Rao, Z. Xu, E. Jang, M. Khansari, and Y. Bai. Retinagan: An object-aware approach to sim-to-real transfer. *arXiv preprint arXiv: Arxiv-2011.03148*, 2020.
- [45] S. Koos, J.-B. Mouret, and S. Doncieux. Crossing the reality gap in evolutionary robotics by promoting transferable controllers. In *Proceedings of the 12th Annual Conference on Genetic and Evolutionary Computation*, GECCO ’10, page 119–126, New York, NY, USA, 2010. Association for Computing Machinery. ISBN 9781450300728. doi:10.1145/1830483.1830505. URL <https://doi.org/10.1145/1830483.1830505>.
- [46] Z. Xie, G. Berseth, P. Clary, J. Hurst, and M. van de Panne. Feedback control for cassie with deep reinforcement learning. *arXiv preprint arXiv: Arxiv-1803.05580*, 2018.
- [47] R. Martín-Martín, M. A. Lee, R. Gardner, S. Savarese, J. Bohg, and A. Garg. Variable impedance control in end-effector space: An action space for reinforcement learning in contact-rich tasks. *arXiv preprint arXiv: Arxiv-1906.08880*, 2019.
- [48] J. Wong, V. Makoviychuk, A. Anandkumar, and Y. Zhu. Oscar: Data-driven operational space control for adaptive and robust robot manipulation. *arXiv preprint arXiv: Arxiv-2110.00704*, 2021.
- [49] E. Aljalbout, F. Frank, M. Karl, and P. van der Smagt. On the role of the action space in robot manipulation learning and sim-to-real transfer. *arXiv preprint arXiv: Arxiv-2312.03673*, 2023.
- [50] Y. S. Narang, K. Storey, I. Akinola, M. Macklin, P. Reist, L. Wawrzyniak, Y. Guo, Á. Moravánszky, G. State, M. Lu, A. Handa, and D. Fox. Factory: Fast contact for robotic assembly. In K. Hauser, D. A. Shell, and S. Huang, editors, *Robotics: Science and Systems XVIII, New York City, NY, USA, June 27 - July 1, 2022*, 2022. doi:10.15607/RSS.2022.XVIII.035. URL <https://doi.org/10.15607/RSS.2022.XVIII.035>.
- [51] L. Ljung. *System Identification*, pages 163–173. Birkhäuser Boston, Boston, MA, 1998. ISBN 978-1-4612-1768-8. doi:10.1007/978-1-4612-1768-8\_11. URL [https://doi.org/10.1007/978-1-4612-1768-8\\_11](https://doi.org/10.1007/978-1-4612-1768-8_11).
- [52] P. Chang and T. Padir. Sim2real2sim: Bridging the gap between simulation and real-world in flexible object manipulation. *arXiv preprint arXiv: Arxiv-2002.02538*, 2020.

- [53] X. B. Peng, M. Andrychowicz, W. Zaremba, and P. Abbeel. Sim-to-real transfer of robotic control with dynamics randomization. *arXiv preprint arXiv: Arxiv-1710.06537*, 2017.
- [54] A. Handa, A. Allshire, V. Makoviychuk, A. Petrenko, R. Singh, J. Liu, D. Makoviichuk, K. V. Wyk, A. Zhurkevich, B. Sundaralingam, and Y. S. Narang. Dextreme: Transfer of agile in-hand manipulation from simulation to reality. In *IEEE International Conference on Robotics and Automation, ICRA 2023, London, UK, May 29 - June 2, 2023*, pages 5977–5984. IEEE, 2023. doi:[10.1109/ICRA48891.2023.10160216](https://doi.org/10.1109/ICRA48891.2023.10160216). URL <https://doi.org/10.1109/ICRA48891.2023.10160216>.
- [55] J. Wang, Y. Qin, K. Kuang, Y. Korkmaz, A. Gurumoorthy, H. Su, and X. Wang. Cyberdemo: Augmenting simulated human demonstration for real-world dexterous manipulation. *arXiv preprint arXiv: Arxiv-2402.14795*, 2024.
- [56] G. Schoettler, A. Nair, J. A. Ojea, S. Levine, and E. Solowjow. Meta-reinforcement learning for robotic industrial insertion tasks. *arXiv preprint arXiv: Arxiv-2004.14404*, 2020.
- [57] Y. Zhang, L. Ke, A. Deshpande, A. Gupta, and S. Srinivasa. Cherry-Picking with Reinforcement Learning. In *Proceedings of Robotics: Science and Systems*, Daegu, Republic of Korea, July 2023. doi:[10.15607/RSS.2023.XIX.021](https://doi.org/10.15607/RSS.2023.XIX.021).
- [58] Y. Chebotar, A. Handa, V. Makoviychuk, M. Macklin, J. Issac, N. D. Ratliff, and D. Fox. Closing the sim-to-real loop: Adapting simulation randomization with real world experience. In *International Conference on Robotics and Automation, ICRA 2019, Montreal, QC, Canada, May 20-24, 2019*, pages 8973–8979. IEEE, 2019. doi:[10.1109/ICRA.2019.8793789](https://doi.org/10.1109/ICRA.2019.8793789). URL <https://doi.org/10.1109/ICRA.2019.8793789>.
- [59] J. P. Hanna and P. Stone. Grounded action transformation for robot learning in simulation. In *Proceedings of the Thirty-First AAAI Conference on Artificial Intelligence, AAAI’17*, page 4931–4932. AAAI Press, 2017.
- [60] E. Heiden, D. Millard, E. Coumans, and G. S. Sukhatme. Augmenting differentiable simulators with neural networks to close the sim2real gap. *arXiv preprint arXiv: Arxiv-2007.06045*, 2020.
- [61] C. A. Cruz and T. Igarashi. A survey on interactive reinforcement learning: Design principles and open challenges. *arXiv preprint arXiv: Arxiv-2105.12949*, 2021.
- [62] Y. Cui, P. Koppol, H. Admoni, S. Niekum, R. Simmons, A. Steinfeld, and T. Fitzgerald. Understanding the relationship between interactions and outcomes in human-in-the-loop machine learning. In Z.-H. Zhou, editor, *Proceedings of the Thirtieth International Joint Conference on Artificial Intelligence, IJCAI-21*, pages 4382–4391. International Joint Conferences on Artificial Intelligence Organization, 8 2021. doi:[10.24963/ijcai.2021/599](https://doi.org/10.24963/ijcai.2021/599). URL <https://doi.org/10.24963/ijcai.2021/599>. Survey Track.
- [63] R. Zhang, F. Torabi, L. Guan, D. H. Ballard, and P. Stone. Leveraging human guidance for deep reinforcement learning tasks. *arXiv preprint arXiv: Arxiv-1909.09906*, 2019.
- [64] S. Javdani, S. S. Srinivasa, and J. A. Bagnell. Shared autonomy via hindsight optimization. *arXiv preprint arXiv: Arxiv-1503.07619*, 2015.
- [65] S. Reddy, A. D. Dragan, and S. Levine. Shared autonomy via deep reinforcement learning. *arXiv preprint arXiv: Arxiv-1802.01744*, 2018.
- [66] M. Kelly, C. Sidrane, K. Driggs-Campbell, and M. J. Kochenderfer. Hg-dagger: Interactive imitation learning with human experts. *arXiv preprint arXiv: Arxiv-1810.02890*, 2018.
- [67] A. Mandlekar, D. Xu, R. Martín-Martín, Y. Zhu, L. Fei-Fei, and S. Savarese. Human-in-the-loop imitation learning using remote teleoperation. *arXiv preprint arXiv: Arxiv-2012.06733*, 2020.

- [68] A. Mandlekar, D. Xu, J. Wong, S. Nasiriany, C. Wang, R. Kulkarni, L. Fei-Fei, S. Savarese, Y. Zhu, and R. Martín-Martín. What matters in learning from offline human demonstrations for robot manipulation. *arXiv preprint arXiv: Arxiv-2108.03298*, 2021.
- [69] I. Kostrikov, A. Nair, and S. Levine. Offline reinforcement learning with implicit q-learning. *arXiv preprint arXiv: Arxiv-2110.06169*, 2021.
- [70] H. Liu, S. Nasiriany, L. Zhang, Z. Bao, and Y. Zhu. Robot learning on the job: Human-in-the-loop autonomy and learning during deployment. *arXiv preprint arXiv: Arxiv-2211.08416*, 2022.
- [71] A. Abdolmaleki, J. T. Springenberg, Y. Tassa, R. Munos, N. Heess, and M. Riedmiller. Maximum a posteriori policy optimisation. *arXiv preprint arXiv: Arxiv-1806.06920*, 2018.
- [72] D. A. Pomerleau. Alvinn: An autonomous land vehicle in a neural network. In D. Touretzky, editor, *Advances in Neural Information Processing Systems*, volume 1. Morgan-Kaufmann, 1988. URL [https://proceedings.neurips.cc/paper\\_files/paper/1988/file/812b4ba287f5ee0bc9d43bbf5bbe87fb-Paper.pdf](https://proceedings.neurips.cc/paper_files/paper/1988/file/812b4ba287f5ee0bc9d43bbf5bbe87fb-Paper.pdf).
- [73] Y. Zhu, Z. Wang, J. Merel, A. Rusu, T. Erez, S. Cabi, S. Tunyasuvunakool, J. Kramár, R. Hadsell, N. de Freitas, and N. Heess. Reinforcement and imitation learning for diverse visuomotor skills. *arXiv preprint arXiv: Arxiv-1802.09564*, 2018.
- [74] A. Xie, L. Lee, T. Xiao, and C. Finn. Decomposing the generalization gap in imitation learning for visual robotic manipulation. *arXiv preprint arXiv: Arxiv-2307.03659*, 2023.
- [75] Y. Qin, B. Huang, Z.-H. Yin, H. Su, and X. Wang. Dexpoint: Generalizable point cloud reinforcement learning for sim-to-real dexterous manipulation. *arXiv preprint arXiv: Arxiv-2211.09423*, 2022.
- [76] O. Khatib. A unified approach for motion and force control of robot manipulators: The operational space formulation. *IEEE Journal on Robotics and Automation*, 3(1):43–53, 1987. doi:[10.1109/JRA.1987.1087068](https://doi.org/10.1109/JRA.1987.1087068).
- [77] J. Nakanishi, R. Cory, M. Mistry, J. Peters, and S. Schaal. Operational space control: A theoretical and empirical comparison. *The International Journal of Robotics Research*, 27(6):737–757, 2008. doi:[10.1177/0278364908091463](https://doi.org/10.1177/0278364908091463). URL <https://doi.org/10.1177/0278364908091463>.
- [78] A. A. Rusu, S. G. Colmenarejo, C. Gulcehre, G. Desjardins, J. Kirkpatrick, R. Pascanu, V. Mnih, K. Kavukcuoglu, and R. Hadsell. Policy distillation. *arXiv preprint arXiv: Arxiv-1511.06295*, 2015.
- [79] T. Chen, M. Tippur, S. Wu, V. Kumar, E. Adelson, and P. Agrawal. Visual dexterity: In-hand dexterous manipulation from depth. *arXiv preprint arXiv: Arxiv-2211.11744*, 2022.
- [80] T. Chen, J. Xu, and P. Agrawal. A system for general in-hand object re-orientation. In A. Faust, D. Hsu, and G. Neumann, editors, *Conference on Robot Learning, 8-11 November 2021, London, UK*, volume 164 of *Proceedings of Machine Learning Research*, pages 297–307. PMLR, 2021. URL <https://proceedings.mlr.press/v164/chen22a.html>.
- [81] T. Johannink, S. Bahl, A. Nair, J. Luo, A. Kumar, M. Loskyll, J. A. Ojea, E. Solowjow, and S. Levine. Residual reinforcement learning for robot control. *arXiv preprint arXiv: Arxiv-1812.03201*, 2018.
- [82] T. Silver, K. Allen, J. Tenenbaum, and L. Kaelbling. Residual policy learning. *arXiv preprint arXiv: Arxiv-1812.06298*, 2018.
- [83] A. Zeng, S. Song, J. Lee, A. Rodriguez, and T. Funkhouser. Tossingbot: Learning to throw arbitrary objects with residual physics. *arXiv preprint arXiv: Arxiv-1903.11239*, 2019.

- [84] J. Schulman, F. Wolski, P. Dhariwal, A. Radford, and O. Klimov. Proximal policy optimization algorithms. *arXiv preprint arXiv: Arxiv-1707.06347*, 2017.
- [85] C. Chi, S. Feng, Y. Du, Z. Xu, E. Cousineau, B. Burchfiel, and S. Song. Diffusion policy: Visuomotor policy learning via action diffusion. In K. E. Bekris, K. Hauser, S. L. Herbert, and J. Yu, editors, *Robotics: Science and Systems XIX, Daegu, Republic of Korea, July 10-14, 2023*, 2023. doi:10.15607/RSS.2023.XIX.026. URL <https://doi.org/10.15607/RSS.2023.XIX.026>.
- [86] C. R. Qi, H. Su, K. Mo, and L. J. Guibas. Pointnet: Deep learning on point sets for 3d classification and segmentation. *arXiv preprint arXiv: Arxiv-1612.00593*, 2016.
- [87] A. Jaegle, F. Gimeno, A. Brock, A. Zisserman, O. Vinyals, and J. Carreira. Perceiver: General perception with iterative attention. *arXiv preprint arXiv: Arxiv-2103.03206*, 2021.
- [88] J. Lee, Y. Lee, J. Kim, A. R. Kosiorek, S. Choi, and Y. W. Teh. Set transformer: A framework for attention-based permutation-invariant neural networks. *arXiv preprint arXiv: Arxiv-1810.00825*, 2018.
- [89] I. Loshchilov and F. Hutter. Sgdr: Stochastic gradient descent with warm restarts. *arXiv preprint arXiv: Arxiv-1608.03983*, 2016.
- [90] M. Heo, Y. Lee, D. Lee, and J. J. Lim. Furniturebench: Reproducible real-world benchmark for long-horizon complex manipulation. In K. E. Bekris, K. Hauser, S. L. Herbert, and J. Yu, editors, *Robotics: Science and Systems XIX, Daegu, Republic of Korea, July 10-14, 2023*, 2023. doi:10.15607/RSS.2023.XIX.041. URL <https://doi.org/10.15607/RSS.2023.XIX.041>.
- [91] A. Fishman, A. Murali, C. Eppner, B. Peele, B. Boots, and D. Fox. Motion policy networks. In K. Liu, D. Kulic, and J. Ichnowski, editors, *Conference on Robot Learning, CoRL 2022, 14-18 December 2022, Auckland, New Zealand*, volume 205 of *Proceedings of Machine Learning Research*, pages 967–977. PMLR, 2022. URL <https://proceedings.mlr.press/v205/fishman23a.html>.
- [92] R. Hoque, A. Balakrishna, E. Novoseller, A. Wilcox, D. S. Brown, and K. Goldberg. Thriftydagger: Budget-aware novelty and risk gating for interactive imitation learning. *arXiv preprint arXiv: Arxiv-2109.08273*, 2021.
- [93] R. Tedrake and the Drake Development Team. Drake: Model-based design and verification for robotics, 2019. URL <https://drake.mit.edu>.
- [94] F. Xiang, Y. Qin, K. Mo, Y. Xia, H. Zhu, F. Liu, M. Liu, H. Jiang, Y. Yuan, H. Wang, L. Yi, A. X. Chang, L. J. Guibas, and H. Su. Sapien: A simulated part-based interactive environment. *arXiv preprint arXiv: Arxiv-2003.08515*, 2020.
- [95] M. Mittal, C. Yu, Q. Yu, J. Liu, N. Rudin, D. Hoeller, J. L. Yuan, P. P. Tehrani, R. Singh, Y. Guo, H. Mazhar, A. Mandlekar, B. Babich, G. State, M. Hutter, and A. Garg. Orbit: A unified simulation framework for interactive robot learning environments. *arXiv preprint arXiv: Arxiv-2301.04195*, 2023.
- [96] A. Zeng, P. Florence, J. Tompson, S. Welker, J. Chien, M. Attarian, T. Armstrong, I. Krasin, D. Duong, A. Wahid, V. Sindhwani, and J. Lee. Transporter networks: Rearranging the visual world for robotic manipulation. *arXiv preprint arXiv: Arxiv-2010.14406*, 2020.
- [97] M. Shridhar, L. Manuelli, and D. Fox. Cliport: What and where pathways for robotic manipulation. *arXiv preprint arXiv: Arxiv-2109.12098*, 2021.
- [98] Y. Jiang, A. Gupta, Z. Zhang, G. Wang, Y. Dou, Y. Chen, L. Fei-Fei, A. Anandkumar, Y. Zhu, and L. Fan. Vima: General robot manipulation with multimodal prompts. *arXiv preprint arXiv: Arxiv-2210.03094*, 2022.

- [99] M. Shridhar, L. Manuelli, and D. Fox. Perceiver-actor: A multi-task transformer for robotic manipulation. *arXiv preprint arXiv: Arxiv-2209.05451*, 2022.
- [100] D. Batra, A. X. Chang, S. Chernova, A. J. Davison, J. Deng, V. Koltun, S. Levine, J. Malik, I. Mordatch, R. Mottaghi, M. Savva, and H. Su. Rearrangement: A challenge for embodied ai. *arXiv preprint arXiv: Arxiv-2011.01975*, 2020.
- [101] J. Gu, D. S. Chaplot, H. Su, and J. Malik. Multi-skill mobile manipulation for object rearrangement. *arXiv preprint arXiv: Arxiv-2209.02778*, 2022.
- [102] S. Yenamandra, A. Ramachandran, K. Yadav, A. Wang, M. Khanna, T. Gervet, T.-Y. Yang, V. Jain, A. W. Clegg, J. Turner, Z. Kira, M. Savva, A. Chang, D. S. Chaplot, D. Batra, R. Mottaghi, Y. Bisk, and C. Paxton. Homerobot: Open-vocabulary mobile manipulation. *arXiv preprint arXiv: Arxiv-2306.11565*, 2023.
- [103] K. Ehsani, T. Gupta, R. Hendrix, J. Salvador, L. Weihs, K.-H. Zeng, K. P. Singh, Y. Kim, W. Han, A. Herrasti, R. Krishna, D. Schwenk, E. VanderBilt, and A. Kembhavi. Imitating shortest paths in simulation enables effective navigation and manipulation in the real world. *arXiv preprint arXiv: Arxiv-2312.02976*, 2023.
- [104] Y. Wu, W. Yan, T. Kurutach, L. Pinto, and P. Abbeel. Learning to manipulate deformable objects without demonstrations. *arXiv preprint arXiv: Arxiv-1910.13439*, 2019.
- [105] H. Ha and S. Song. Flingbot: The unreasonable effectiveness of dynamic manipulation for cloth unfolding. *arXiv preprint arXiv: Arxiv-2105.03655*, 2021.
- [106] D. Seita, Y. Wang, S. J. Shetty, E. Y. Li, Z. Erickson, and D. Held. Toolflownet: Robotic manipulation with tools via predicting tool flow from point clouds. *arXiv preprint arXiv: Arxiv-2211.09006*, 2022.
- [107] X. Lin, Z. Huang, Y. Li, J. B. Tenenbaum, D. Held, and C. Gan. Diffskill: Skill abstraction from differentiable physics for deformable object manipulations with tools. *arXiv preprint arXiv: Arxiv-2203.17275*, 2022.
- [108] Y. Ji, Z. Li, Y. Sun, X. B. Peng, S. Levine, G. Berseth, and K. Sreenath. Hierarchical reinforcement learning for precise soccer shooting skills using a quadrupedal robot. *arXiv preprint arXiv: Arxiv-2208.01160*, 2022.
- [109] Y. J. Ma, W. Liang, G. Wang, D.-A. Huang, O. Bastani, D. Jayaraman, Y. Zhu, L. Fan, and A. Anandkumar. Eureka: Human-level reward design via coding large language models. *arXiv preprint arXiv: Arxiv-2310.12931*, 2023.
- [110] A. Boeing and T. Bräunl. Leveraging multiple simulators for crossing the reality gap. In *2012 12th International Conference on Control Automation Robotics & Vision (ICARCV)*, pages 1113–1119, 2012. doi:[10.1109/ICARCV.2012.6485313](https://doi.org/10.1109/ICARCV.2012.6485313).
- [111] J. Hwangbo, J. Lee, A. Dosovitskiy, D. Bellicoso, V. Tsounis, V. Koltun, and M. Hutter. Learning agile and dynamic motor skills for legged robots. *Science Robotics*, 4(26):eaau5872, 2019. doi:[10.1126/scirobotics.aau5872](https://doi.org/10.1126/scirobotics.aau5872). URL <https://www.science.org/doi/abs/10.1126/scirobotics.aau5872>.
- [112] J. Luo, E. Solowjow, C. Wen, J. A. Ojea, A. M. Agogino, A. Tamar, and P. Abbeel. Reinforcement learning on variable impedance controller for high-precision robotic assembly. In *International Conference on Robotics and Automation, ICRA 2019, Montreal, QC, Canada, May 20-24, 2019*, pages 3080–3087. IEEE, 2019. doi:[10.1109/ICRA.2019.8793506](https://doi.org/10.1109/ICRA.2019.8793506). URL <https://doi.org/10.1109/ICRA.2019.8793506>.
- [113] P. C. Horak and J. C. Trinkle. On the similarities and differences among contact models in robot simulation. *IEEE Robotics and Automation Letters*, 4(2):493–499, 2019. doi:[10.1109/LRA.2019.2891085](https://doi.org/10.1109/LRA.2019.2891085).

- [114] C. Finn, P. Abbeel, and S. Levine. Model-agnostic meta-learning for fast adaptation of deep networks. *arXiv preprint arXiv: Arxiv-1703.03400*, 2017.
- [115] J. A. Fails and D. R. Olsen. Interactive machine learning. In *Proceedings of the 8th International Conference on Intelligent User Interfaces*, IUI '03, page 39–45, New York, NY, USA, 2003. Association for Computing Machinery. ISBN 1581135866. doi:10.1145/604045.604056. URL <https://doi.org/10.1145/604045.604056>.
- [116] S. Amershi, M. Cakmak, W. B. Knox, and T. Kulesza. Power to the people: The role of humans in interactive machine learning. *AI Magazine*, 35(4):105–120, Dec. 2014. doi:10.1609/aimag.v35i4.2513. URL <https://ojs.aaai.org/aimagazine/index.php/aimagazine/article/view/2513>.
- [117] Y. Yue, J. Broder, R. Kleinberg, and T. Joachims. The k-armed dueling bandits problem. *Journal of Computer and System Sciences*, 78(5):1538–1556, 2012. ISSN 0022-0000. doi:<https://doi.org/10.1016/j.jcss.2011.12.028>. URL <https://www.sciencedirect.com/science/article/pii/S0022000012000281>. JCSS Special Issue: Cloud Computing 2011.
- [118] A. Jain, B. Wojcik, T. Joachims, and A. Saxena. Learning trajectory preferences for manipulators via iterative improvement. *arXiv preprint arXiv: Arxiv-1306.6294*, 2013.
- [119] P. Christiano, J. Leike, T. B. Brown, M. Martic, S. Legg, and D. Amodei. Deep reinforcement learning from human preferences. *arXiv preprint arXiv: Arxiv-1706.03741*, 2017.
- [120] E. Büyük, D. P. Losey, M. Palan, N. C. Landolfi, G. Shevchuk, and D. Sadigh. Learning reward functions from diverse sources of human feedback: Optimally integrating demonstrations and preferences. *arXiv preprint arXiv: Arxiv-2006.14091*, 2020.
- [121] K. Lee, L. Smith, and P. Abbeel. Pebble: Feedback-efficient interactive reinforcement learning via relabeling experience and unsupervised pre-training. *arXiv preprint arXiv: Arxiv-2106.05091*, 2021.
- [122] X. Wang, K. Lee, K. Hakhamaneshi, P. Abbeel, and M. Laskin. Skill preferences: Learning to extract and execute robotic skills from human feedback. *arXiv preprint arXiv: Arxiv-2108.05382*, 2021.
- [123] L. Ouyang, J. Wu, X. Jiang, D. Almeida, C. L. Wainwright, P. Mishkin, C. Zhang, S. Agarwal, K. Slama, A. Ray, J. Schulman, J. Hilton, F. Kelton, L. Miller, M. Simens, A. Askell, P. Welinder, P. Christiano, J. Leike, and R. Lowe. Training language models to follow instructions with human feedback. *arXiv preprint arXiv: Arxiv-2203.02155*, 2022.
- [124] V. Myers, E. Büyük, and D. Sadigh. Active reward learning from online preferences. *arXiv preprint arXiv: Arxiv-2302.13507*, 2023.
- [125] R. Rafailov, A. Sharma, E. Mitchell, S. Ermon, C. D. Manning, and C. Finn. Direct preference optimization: Your language model is secretly a reward model. *arXiv preprint arXiv: Arxiv-2305.18290*, 2023.
- [126] J. Hejna, R. Rafailov, H. Sikchi, C. Finn, S. Niekum, W. B. Knox, and D. Sadigh. Contrastive preference learning: Learning from human feedback without rl. *arXiv preprint arXiv: Arxiv-2310.13639*, 2023.
- [127] W. B. Knox and P. Stone. Reinforcement learning from human reward: Discounting in episodic tasks. In *2012 IEEE RO-MAN: The 21st IEEE International Symposium on Robot and Human Interactive Communication*, pages 878–885, 2012. doi:10.1109/ROMAN.2012.6343862.

- [128] B. D. Argall, E. L. Sauser, and A. G. Billard. Tactile guidance for policy refinement and reuse. In *2010 IEEE 9th International Conference on Development and Learning*, pages 7–12, 2010. doi:[10.1109/DEVLRN.2010.5578872](https://doi.org/10.1109/DEVLRN.2010.5578872).
- [129] T. Fitzgerald, E. Short, A. Goel, and A. Thomaz. Human-guided trajectory adaptation for tool transfer. In *Proceedings of the 18th International Conference on Autonomous Agents and MultiAgent Systems*, AAMAS ’19, page 1350–1358, Richland, SC, 2019. International Foundation for Autonomous Agents and Multiagent Systems. ISBN 9781450363099.
- [130] A. V. Bajcsy, D. P. Losey, M. K. O’Malley, and A. D. Dragan. Learning robot objectives from physical human interaction. In *Conference on Robot Learning*, 2017. URL <https://api.semanticscholar.org/CorpusID:28406224>.
- [131] A. Najar, O. Sigaud, and M. Chetouani. Interactively shaping robot behaviour with unlabeled human instructions. *arXiv preprint arXiv: Arxiv-1902.01670*, 2019.
- [132] N. Wilde, E. Biyik, D. Sadigh, and S. L. Smith. Learning reward functions from scale feedback. *arXiv preprint arXiv: Arxiv-2110.00284*, 2021.
- [133] J. Zhang and K. Cho. Query-efficient imitation learning for end-to-end autonomous driving. *arXiv preprint arXiv: Arxiv-1605.06450*, 2016.
- [134] W. Saunders, G. Sastry, A. Stuhlmuller, and O. Evans. Trial without error: Towards safe reinforcement learning via human intervention. *arXiv preprint arXiv: Arxiv-1707.05173*, 2017.
- [135] Z. Wang, X. Xiao, B. Liu, G. Warnell, and P. Stone. Appli: Adaptive planner parameter learning from interventions. *arXiv preprint arXiv: Arxiv-2011.00400*, 2020.
- [136] C. Celemin and J. R. del Solar. An interactive framework for learning continuous actions policies based on corrective feedback. *Journal of Intelligent & Robotic Systems*, 95:77–97, 2018. doi:[10.1007/s10846-018-0839-z](https://doi.org/10.1007/s10846-018-0839-z). URL <http://link.springer.com/article/10.1007/s10846-018-0839-z/fulltext.html>.
- [137] Z. Peng, W. Mo, C. Duan, Q. Li, and B. Zhou. Learning from active human involvement through proxy value propagation. In *Thirty-seventh Conference on Neural Information Processing Systems*, 2023. URL <https://openreview.net/forum?id=q8SukwaEBy>.
- [138] C. Celemin, R. Pérez-Dattari, E. Chisari, G. Franzese, L. de Souza Rosa, R. Prakash, Z. Ajanović, M. Ferraz, A. Valada, and J. Kober. Interactive imitation learning in robotics: A survey. *arXiv preprint arXiv: Arxiv-2211.00600*, 2022.
- [139] R. Hoque, A. Mandlekar, C. R. Garrett, K. Goldberg, and D. Fox. Interventional data generation for robust and data-efficient robot imitation learning. In *First Workshop on Out-of-Distribution Generalization in Robotics at CoRL 2023*, 2023. URL <https://openreview.net/forum?id=ckFRo0aA3n>.
- [140] J. Crandall and M. Goodrich. Characterizing efficiency of human robot interaction: a case study of shared-control teleoperation. In *IEEE/RSJ International Conference on Intelligent Robots and Systems*, volume 2, pages 1290–1295 vol.2, 2002. doi:[10.1109/IRDS.2002.1043932](https://doi.org/10.1109/IRDS.2002.1043932).
- [141] A. D. Dragan and S. S. Srinivasa. A policy-blending formalism for shared control. *The International Journal of Robotics Research*, 32(7):790–805, 2013. doi:[10.1177/0278364913490324](https://doi.org/10.1177/0278364913490324). URL <https://doi.org/10.1177/0278364913490324>.
- [142] D. Gopinath, S. Jain, and B. D. Argall. Human-in-the-loop optimization of shared autonomy in assistive robotics. *IEEE Robotics and Automation Letters*, 2(1):247–254, 2017. doi:[10.1109/LRA.2016.2593928](https://doi.org/10.1109/LRA.2016.2593928).

- [143] A. D. Dragan and S. S. Srinivasa. *Formalizing assistive teleoperation*, volume 376. MIT Press, July, 2012.
- [144] H. J. Jeon, D. P. Losey, and D. Sadigh. Shared autonomy with learned latent actions. *arXiv preprint arXiv: Arxiv-2005.03210*, 2020.
- [145] Y. Cui, S. Karamcheti, R. Palletti, N. Shivakumar, P. Liang, and D. Sadigh. "no, to the right" – online language corrections for robotic manipulation via shared autonomy. *arXiv preprint arXiv: Arxiv-2301.02555*, 2023.
- [146] P. Wu, Y. Shentu, Z. Yi, X. Lin, and P. Abbeel. Gello: A general, low-cost, and intuitive teleoperation framework for robot manipulators. *arXiv preprint arXiv: Arxiv-2309.13037*, 2023.
- [147] C. Wang, H. Shi, W. Wang, R. Zhang, L. Fei-Fei, and C. K. Liu. Dexcap: Scalable and portable mocap data collection system for dexterous manipulation. *arXiv preprint arXiv: Arxiv-2403.07788*, 2024.
- [148] Z. Fu, T. Z. Zhao, and C. Finn. Mobile aloha: Learning bimanual mobile manipulation with low-cost whole-body teleoperation. *arXiv preprint arXiv: Arxiv-2401.02117*, 2024.
- [149] S. Dass, W. Ai, Y. Jiang, S. Singh, J. Hu, R. Zhang, P. Stone, B. AbbateMatteo, and R. Martín-Martín. Telemoma: A modular and versatile teleoperation system for mobile manipulation. *arXiv preprint arXiv: Arxiv-2403.07869*, 2024.
- [150] T. He, Z. Luo, W. Xiao, C. Zhang, K. Kitani, C. Liu, and G. Shi. Learning human-to-humanoid real-time whole-body teleoperation. *arXiv preprint arXiv: Arxiv-2403.04436*, 2024.
- [151] H. Liu, S. Dass, R. Martín-Martín, and Y. Zhu. Model-based runtime monitoring with interactive imitation learning. *arXiv preprint arXiv: Arxiv-2310.17552*, 2023.
- [152] Z. Liu, A. Bahety, and S. Song. Reflect: Summarizing robot experiences for failure explanation and correction. *arXiv preprint arXiv: Arxiv-2306.15724*, 2023.
- [153] L. Ankile, A. Simeonov, I. Shenfeld, and P. Agrawal. Juicer: Data-efficient imitation learning for robotic assembly. *arXiv preprint arXiv: Arxiv-2404.03729*, 2024.
- [154] M. N. Mistry and L. Righetti. Operational space control of constrained and underactuated systems. In *Robotics: Science and Systems*, 2011. URL <https://api.semanticscholar.org/CorpusID:10392712>.
- [155] L. Fan, G. Wang, Y. Jiang, A. Mandlekar, Y. Yang, H. Zhu, A. Tang, D.-A. Huang, Y. Zhu, and A. Anandkumar. Minedojo: Building open-ended embodied agents with internet-scale knowledge. *arXiv preprint arXiv: Arxiv-2206.08853*, 2022.
- [156] D.-A. Clevert, T. Unterthiner, and S. Hochreiter. Fast and accurate deep network learning by exponential linear units (elus). *arXiv preprint arXiv: Arxiv-1511.07289*, 2015.
- [157] D. Makoviichuk and V. Makoviychuk. rl-games: A high-performance framework for reinforcement learning. [https://github.com/Denys88/rl\\_games](https://github.com/Denys88/rl_games), May 2021.
- [158] J. Schulman, P. Moritz, S. Levine, M. Jordan, and P. Abbeel. High-dimensional continuous control using generalized advantage estimation. *arXiv preprint arXiv: Arxiv-1506.02438*, 2015.
- [159] D. P. Kingma and J. Ba. Adam: A method for stochastic optimization. *arXiv preprint arXiv: Arxiv-1412.6980*, 2014.

- [160] S. Hochreiter and J. Schmidhuber. Long short-term memory. *Neural Comput.*, 9(8):1735–1780, nov 1997. ISSN 0899-7667. doi:10.1162/neco.1997.9.8.1735. URL <https://doi.org/10.1162/neco.1997.9.8.1735>.
- [161] D. Hendrycks and K. Gimpel. Gaussian error linear units (gelus). *arXiv preprint arXiv: Arxiv-1606.08415*, 2016.
- [162] Y. Zhu, A. Joshi, P. Stone, and Y. Zhu. Viola: Imitation learning for vision-based manipulation with object proposal priors. *6th Annual Conference on Robot Learning*, 2022.
- [163] C. R. Qi, L. Yi, H. Su, and L. J. Guibas. Pointnet++: Deep hierarchical feature learning on point sets in a metric space. *arXiv preprint arXiv: Arxiv-1706.02413*, 2017.
- [164] L. X. Shi, Y. Jiang, J. Grigsby, L. J. Fan, and Y. Zhu. Cross-episodic curriculum for transformer agents. *arXiv preprint arXiv: Arxiv-2310.08549*, 2023.

## A Simulation Training Details

In this section, we provide details about simulation training, including the used simulator backend, task designs, reinforcement learning (RL) training of teacher policy, and student policy distillation.

### A.1 The Simulator

We use Isaac Gym Preview 4 [10] as the simulator backend. NVIDIA PhysX<sup>1</sup> is used as the physics engine to provide realistic and precise simulation. Simulation settings are listed in Table A.I. The robot model is from Franka ROS package<sup>2</sup>. We borrow furniture models from FurnitureBench [90] to create various tasks that require complex and contact-rich manipulation.

Table A.I: **Simulation settings.**

Hyperparameter	Value
Simulation Frequency	60 Hz
Control Frequency	60 Hz
Num Substeps	2
Num Position Iterations	8
Num Velocity Iterations	1

## A.2 Task Implementations

We implement four tasks based on the furniture model `square_table`: *Stabilize*, *Reach and Grasp*, *Insert*, and *Screw*. An overview of simulated tasks is shown in Fig A.1. We elaborate on their initial conditions, success criteria, reward functions, and other necessary information.

### A.2.1 Stabilize

In this task, the robot needs to push the square tabletop to the right corner of the wall such that it is supported and remains stable in following assembly steps. The robot is initialized such that its gripper locates at a neutral position. The tabletop is initialized at the coordinate (0.54, 0.00) relative to the robot base. We then randomly translate it with displacements drawn from  $\mathcal{U}(-0.015, 0.015)$  along x and y directions (the distance unit is meter hereafter). We also apply random Z rotation with values drawn from  $\mathcal{U}(-15^\circ, 15^\circ)$ . Four table legs are initialized in the scene. The task is successful only when the following three conditions are met:

- 1) The square tabletop contacts the front and right walls;
- 2) The square tabletop is within a pre-defined region;
- 3) No table leg is in the pre-defined region.

We use the following reward function:

$$r_t = w_{\text{success}} \mathbb{1}_{\text{success}} - w_{\dot{\mathbf{q}}} \|\dot{\mathbf{q}}_t\| - w_{\text{action}} \|a_t\|, \quad (\text{A.1})$$

where  $w_{\text{success}}$  is the success reward,  $\mathbb{1}_{\text{success}}$  indicates the success according to aforementioned conditions,  $w_{\dot{\mathbf{q}}}$  penalizes large joint velocities,  $\dot{\mathbf{q}}_t$  is the joint velocity,  $w_{\text{action}}$  penalizes large action commands, and  $a_t$  represents the action command at time step  $t$ . We set  $w_{\text{success}} = 10$ ,  $w_{\dot{\mathbf{q}}} = 10^{-5}$ , and  $w_{\text{action}} = 10^{-5}$ . The episode length is 100. One episode terminates upon success or timeout.

### A.2.2 Reach and Grasp

In this task, the robot needs to reach and grasp a table leg that is randomly spawned in the valid workspace region. The task is successful once the robot grasps the table leg and lifts it for a certain

<sup>1</sup><https://developer.nvidia.com/physx-sdk>

<sup>2</sup>[https://github.com/frankaemika/franka\\_ros](https://github.com/frankaemika/franka_ros)

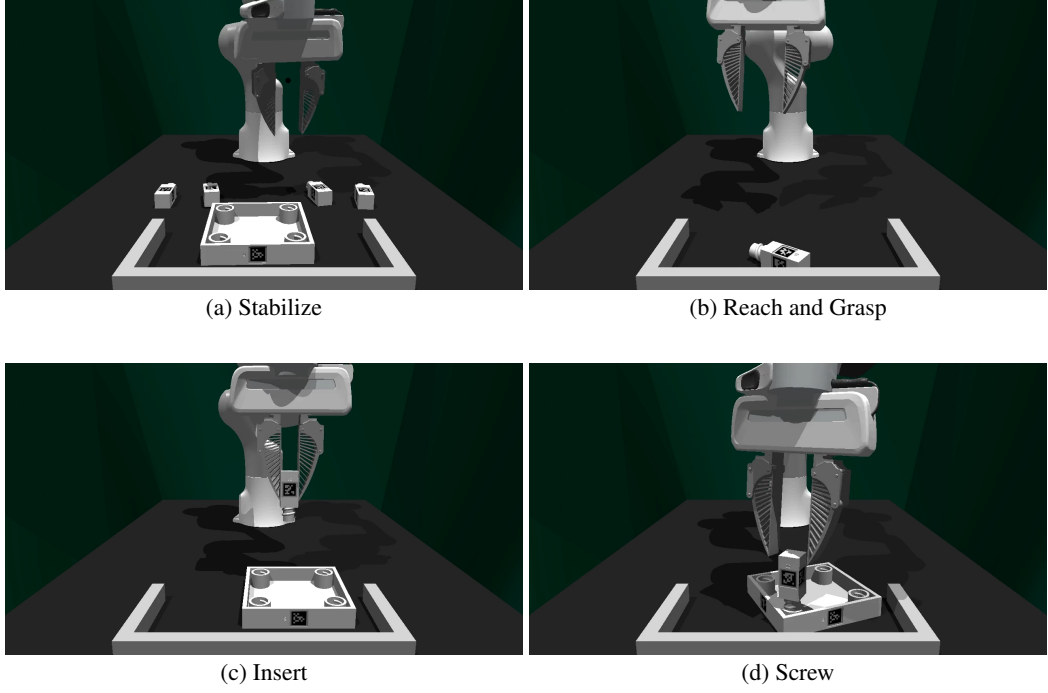


Figure A.1: **Visualization of simulated tasks.**

height. The object’s irregular shape limits certain grasping poses. For example, the end-effector needs to be near orthogonal to the table leg in the  $xy$  plane and far away from the screw thread. Therefore, we design a curriculum over the object geometry to warm up the RL learning. It gradually adjusts the object geometry from a cube, to a cuboid, and finally the table leg. In all curriculum stages, the reward function is

$$r_t = w_{distance}d + w_{lifted}\mathbb{1}_{lifted} + w_{success}\mathbb{1}_{success}. \quad (\text{A.2})$$

Here,  $w_{distance}$  is the weight for distance reward,  $w_{lifted}$  is the reward for the leg being lifted, and  $w_{success}$  is the success weight.  $d$  is the distance to the table leg and is calculated as

$$d = 1 - \tanh\left(\frac{10}{4}(d_{eef} + d_{left.finger} + d_{right.finger} + d_{orthogonal})\right), \quad (\text{A.3})$$

where  $d_{eef}$  is the distance between the end-effector and the table leg,  $d_{left.finger}$  is the distance between the left gripper tip to the table leg,  $d_{right.finger}$  is the distance between the right gripper tip to the table leg, and  $d_{orthogonal}$  is the difference between the current and the orthogonal grasping orientations. We set  $w_{distance} = 0.1$ ,  $w_{lifted} = 1.0$ , and  $w_{success} = 200.0$ . The episode length is 50. One episode terminates upon success or timeout.

### A.2.3 Insert

In this task, the robot needs to insert a pre-grasped table leg into the far right assembly hole of the tabletop, while the tabletop is already stabilized. The tabletop is initialized at the coordinate  $(0.53, 0.05)$  relative to the robot base. We then randomly translate it with displacements sampled from  $\mathcal{U}(-0.02, 0.02)$  along  $x$  and  $y$  directions. We also apply random  $Z$  rotation with values drawn from  $\mathcal{U}(-45^\circ, 45^\circ)$ . We further randomize the robot’s pose by adding noises sampled from  $\mathcal{U}(-0.25, 0.25)$  to joint positions. The task is successful when the table leg remains vertical and is close to the correct assembly position within a small threshold. We design curricula over the randomization strength to facilitate the learning. The following reward function is used:

$$r_t = w_{distance}d + w_{success}\mathbb{1}_{success}, \quad (\text{A.4})$$

where  $w_{distance}$  is the weight for distance-based reward,  $d$  is the distance between the table leg and target assembly position,  $w_{success}$  is the success weight, and  $\mathbb{1}_{success}$  indicates task success. The distance  $d$  consists of an Euclidean distance  $d_{position}$  and an orientation distance  $d_{vertical}$  to encourage the robot to keep the table leg vertical.

$$d = 1 - \tanh\left(\frac{10}{2}d_{position} + d_{vertical}\right) \quad (\text{A.5})$$

We set  $w_{distance} = 1.0$  and  $w_{success} = 100.0$ . The episode length is 100. One episode terminates upon success or timeout.

#### A.2.4 Screw

In this task, the robot is initialized such that its end-effector is close to an inserted table leg. It needs to screw the table leg clockwise into the tabletop. We design curricula over the action space: at the early stage, the robot only controls the end-effector’s orientation; at the latter stage, it gradually takes full control. We slightly randomize object and robot poses during initialization. The reward function is

$$r_t = (1 - \mathbb{1}_{failure})(w_{screw}d_{screw} + w_{success}\mathbb{1}_{success}) - w_{deviation}d_{deviation}. \quad (\text{A.6})$$

Here,  $\mathbb{1}_{failure}$  indicates the task failure,  $w_{screw}$  is the screwing reward weight,  $d_{screw}$  measures the screwed angle,  $w_{success}$  is the success weight, and  $\mathbb{1}_{success}$  indicates the task success. The task is considered as successful when the leg has been screwed  $180^\circ$  into the tabletop. It is considered as failed when the table leg tilts more than  $10^\circ$  from the vertical pose. We set  $w_{screw} = 0.1$ ,  $w_{success} = 100.0$ , and  $w_{deviation} = 10^{-2}$ . The episode length is 200. One episode terminates upon success, failure, or timeout.

### A.3 Teacher Policy Training

#### A.3.1 Model Details

**Observation Space** Besides proprioceptive observations, teacher policies also receive privileged observations to facilitate the learning. They include objects’ states (poses and velocities), end-effector’s velocity, contact forces, gripper left and right fingers’ positions, gripper center position, and joint velocities. Full observations are summarized in Table A.II.

Table A.II: The observation space for teacher policies.

Name	Dimension	Name	Dimension
Proprioceptive		Privileged	
Joint Position	7	Objects States	$N_{objects} \times 13$
Cosine Joint Position	7	End-Effector Velocity	6
Sine Joint Position	7	Contact Forces	$N_{objects} \times 3$
End-Effector Position	3	Left and Right Fingers’ Positions	6
End-Effector Rotation	4	Gripper Center Position	3
Gripper Width	1	Joint Velocity	7

**Controller and Action Space** An operational space controller (OSC) [76] is used in teacher policy training to improve sample efficiency. We follow Mistry and Righetti [154] to add nullspace control torques to prevent large changes in joint configuration. The action space is thus the change of end-effector’s pose. We further add a binary action to control gripper’s opening and closing. Formally, it can be expressed as  $\mathcal{A}_{teacher} = (\delta x, \delta y, \delta z, \delta r, \delta p, \delta y, \mathbb{1}_{gripper})$ , where  $(\delta x, \delta y, \delta z) \in \mathbb{R}^3$  is the translation change,  $(\delta r, \delta p, \delta y) \in \mathbb{R}^3$  is the rotation change, and  $\mathbb{1}_{gripper} \in \{0, 1\}$  is the gripper action.

**Model Architecture** We use feed-forward policies [155] in RL training. It consists of MLP encoders to encode proprioceptive and privileged vector observations, and unimodal Gaussian distributions as the action head. Model hyperparameters are listed in Table A.III.

Table A.III: Model hyperparameters for RL teacher policies.

Hyperparameter	Value	Hyperparameter	Value
Obs. Encoder Hidden Depth	1	Obs. Encoder Activation	ReLU
Obs. Encoder Hidden Dim	256	Action Head Hidden Layers	[256, 128, 64]
Obs. Encoder Output Dim	256	Action Head Activation	ELU [156]

### A.3.2 Domain Randomization

We apply domain randomization during RL training to learn more robust teacher policies. Parameters are summarized in Table A.IV.

Table A.IV: Domain randomization used in RL training.

Parameter	Type	Distribution
<b>Robot</b>		
Mass	Scaling	$\mathcal{U}(0.5, 1.5)$
Friction	Scaling	$\mathcal{U}(0.7, 1.3)$
Joint Lower Limit	Scaling	$\log \mathcal{U}(1.00, 1.01)$
Joint Upper Limit	Scaling	$\log \mathcal{U}(1.00, 1.01)$
Joint Stiffness	Scaling	$\log \mathcal{U}(1.00, 1.01)$
Joint Damping	Scaling	$\log \mathcal{U}(1.00, 1.01)$
<b>Simulation</b>		
Gravity	Additive	$\mathcal{U}(0.0, 0.4)$
<b>Objects</b>		
Mass	Scaling	$\mathcal{U}(0.5, 1.5)$
Friction	Scaling	$\mathcal{U}(0.5, 1.5)$
Rolling Friction	Scaling	$\mathcal{U}(0.5, 1.5)$
Torsion Friction	Scaling	$\mathcal{U}(0.5, 1.5)$
Restitution	Additive	$\mathcal{U}(0.0, 1.0)$
Compliance	Additive	$\mathcal{U}(0.0, 1.0)$

### A.3.3 RL Training Details

We use the model-free RL algorithm Proximal Policy Optimization (PPO) [84] to learn teacher policies. Hyperparameters are listed in Table A.V. We customize the framework from Makoviichuk and Makoviychuk [157] to use as our training framework.

Table A.V: Hyperparameters used in PPO training.

Hyperparameter	Value	Hyperparameter	Value
Learning Rate	$5 \times 10^{-4}$	Critic Weight	4
Discount Factor	0.99	GAE [158] $\lambda$	0.95
Entropy Weight	0	PPO $\epsilon$	0.2
Optimizer	Adam [159]	Horizon	32

## A.4 Student Policy Distillation

### A.4.1 Data Generation

We use trained teacher policies as oracles to generate data for student policies training. Concretely, we roll out each teacher policy to generate 10,000 successful trajectories for each task. We exclude trajectories that are shorter than 20 steps.

#### A.4.2 Observation Space

Student policies receive observations that can be obtained in the real world. They are point-cloud and proprioceptive observations. We synthesize point clouds from objects' 6D poses to improve the training throughput. Concretely, given the groundtruth point cloud of the  $m$ -th object  $\mathbf{P}^{(m)} \in \mathbb{R}^{K \times 3}$ , we transform it into the global frame through  $\mathbf{P}_g^{(m)} = \mathbf{P}^{(m)} (\mathbf{R}^{(m)})^\top + (\mathbf{p}^{(m)})^\top$ . Here  $\mathbf{R}^{(m)} \in \mathbb{R}^{3 \times 3}$  and  $\mathbf{p}^{(m)} \in \mathbb{R}^{3 \times 1}$  denote the object's orientation and translation in the global frame. Further, the point-cloud representation of a scene  $\mathbf{S}$  with  $M$  objects is aggregated as  $\mathbf{P}^{\mathbf{S}} = \bigcup_{m=1}^M \mathbf{P}_g^{(m)}$ . For the robot, we only include point clouds for its two fingers and ignore other parts. To facilitate policies to differentiate gripper fingers from the scene, we extend the coordinate dimension to include a semantic label  $\in \{0, 1\}$  that indicates gripper fingers or not. This information can be obtained on real robots through forward kinematics. A full point cloud is then downsampled to 768 points. Table A.VI lists the observation space.

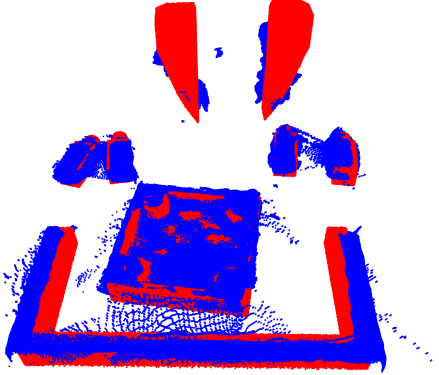


Figure A.2: **Visualization of paired point clouds in simulation (red) and reality (blue).**

Table A.VI: **The observation space for student policies.**

Name	Dimension
Point Cloud	$768 \times 4$
Proprioceptive	
Joint Position	7
Cosine Joint Position	7
Sine Joint Position	7
End-Effector Position	3
End-Effector Rotation	4
Gripper Width	1

#### A.4.3 Action Space Distillation

To reduce the controller sim-to-real gap before transfer, we train student policies to output in the configuration space. To achieve that, we relabel actions  $\hat{a}$  in trajectories generated by teacher policies from end-effector's delta poses to absolute joint positions. This is equivalent to set  $\hat{a}_t = \mathbf{q}_{t+1}$  for all time steps. Therefore, the action space for student policies is  $\mathcal{A}_{student} = (\mathbf{q}, \mathbb{1}_{gripper})$ , where  $\mathbf{q} \in \mathbb{R}^7$  is the joint position within the valid range. In simulation, student policies' actions are deployed with a joint position controller.

#### A.4.4 Model Architecture

We use feed-forward policies for tasks *Reach and Grasp* and *Insert* and recurrent policies for tasks *Stabilize* and *Screw* as we find they achieve the best distillation results. PointNets [86] are used to en-

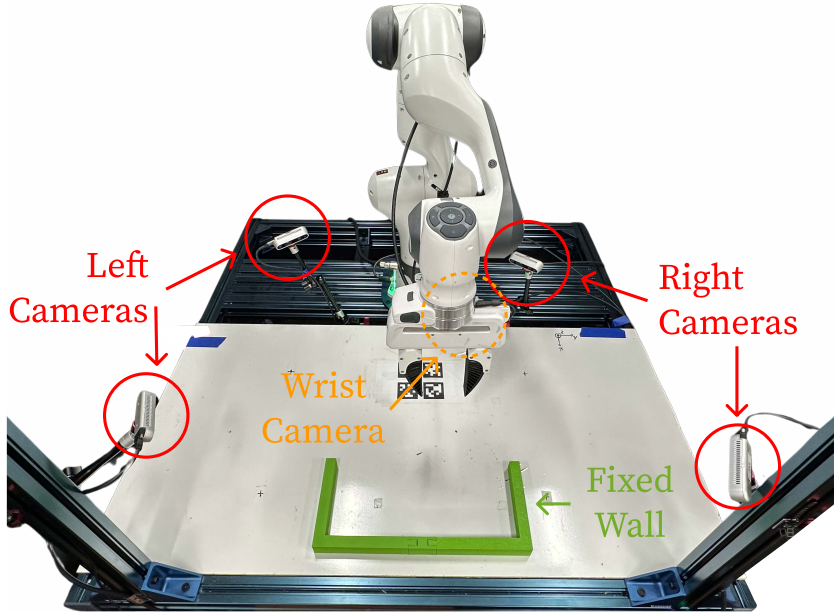


Figure A.3: **System setup.** Our system consists of a Franka Emika 3 robot mounted on the tabletop, four fixed cameras and one wrist camera (positioned at the rear side of the end-effector) for point cloud reconstruction, and a 3d-printed three-sided wall glued onto tabletop to provide external support.

code point clouds. Recall that each point in the point cloud also contains a semantic label indicating the gripper or not. We concatenate point coordinates with these semantic labels’ vector embeddings before passing into the PointNet encoder. We use Gaussian Mixture Models (GMM) [68] as the action head. Detailed model hyperparameters are listed in Table A.VII.

Table A.VII: **Model hyperparameters for student policies.**

Hyperparameter	Value	Hyperparameter	Value
Point Cloud		RNN	
PointNet Hidden Dim	256	RNN Type	LSTM [160]
PointNet Hidden Depth	2	RNN Num Layers	2
PointNet Output Dim	256	RNN Hidden Dim	512
PointNet Activation	GELU [161]	RNN Horizon	5
Gripper Semantic Embd Dim	128	GMM Action Head	
Feature Fusion		Hidden Dim	128
MLP Hidden Dim	512	Hidden Depth	3
MLP Hidden Depth	1	Num Modes	5
MLP Activation	ReLU	Activation	ReLU

#### A.4.5 Data Augmentation

We apply strong data augmentation during distillation. For point-cloud observations, random translation and random jitter are independently applied with a probability  $P_{pcd\_aug} = 0.4$ . We also add Gaussian noises to proprioceptive observations. Augmentation parameters are listed in Table A.VIII.

#### A.4.6 Training Details

To regularize point-cloud features, we separately collect a dataset containing 59 pairs of matched point clouds in simulation and reality. One pair from them is visualized in Fig A.2. Student policies are trained by minimizing Eq. 1, where we set  $\beta = 10^{-3}$ . We use the Adam optimizer [159] with a learning rate of  $10^{-4}$  during training. We periodically roll out student policies in simulation for 1,000 episodes. We then select the checkpoint that corresponds to the highest success rate to use as the base policy in the real-world learning stage.

Table A.VIII: Data augmentation used in distillation.

Hyperparameter	Value
Point Cloud	
Augmentation Probability	0.4
Random Translation Distribution	$\mathcal{U}(-0.04, 0.04)$
Random Jittering Ratio	0.1
Random Jittering Distribution	$\mathcal{N}(0, 0.01)$
Random Jittering Low	-0.015
Random Jittering High	0.015
Proprioception	
Prop. Noise Distribution	$\mathcal{N}(0, 0.1)$
Prop. Noise Low	-0.3
Prop. Noise High	0.3



Figure A.4: A soft gripper that can bend for better grasping.

## B Real-World Learning Details

In this section, we provide details about real-world learning, including the hardware setup, human-in-the-loop data collection, and residual policy training.

### B.1 Hardware Setup

As shown in Fig. A.3, our system consists of a Franka Emika 3 robot mounted on the tabletop. We use four fixed cameras and one wrist camera for point cloud reconstruction. They are three RealSense D435 and two RealSense D415. There is also a 3d-printed three-sided wall glued on top of the table to provide external support. We use a soft gripper for better grasping (Fig A.4). We use a joint position controller from the Deoxys library [162] to control our robot at 1000 Hz.

### B.2 Obtaining Point Clouds from Multi-View Cameras

We use multi-view cameras for point cloud reconstruction to avoid occlusions. Specifically, we first calibrate all cameras to obtain their poses in the robot base frame. We then transform captured point clouds in camera frames to the robot base frame and concatenate them together. We further perform cropping based on coordinates and remove statistical and radius outliers. To identify points belonging to the gripper so that we can add gripper semantic labels (Sec. A.4.2), we compute poses for two gripper fingers through forward kinematics. We then remove measured points corresponding to gripper fingers through K-nearest neighbor, given fingers' poses and synthetic point clouds. Subsequently, we add semantic labels to points belonging to the scene and synthetic gripper's point clouds. Finally, we uniformly down-sample without replacement. We opt to not use farthest point sampling [163] due to its slow speed. One example is shown in Fig. A.5.

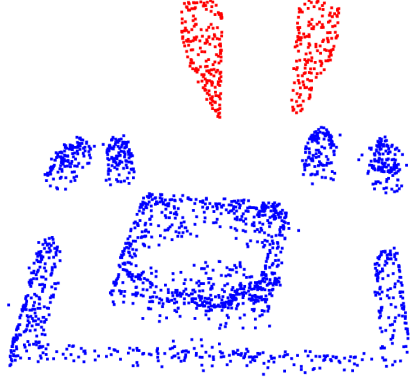


Figure A.5: **Visualization of real-world point-cloud observations.** We obtain them by 1) cropping point clouds fused from multi-view cameras based on coordinates, 2) removing statistical and radius outliers, 3) removing points corresponding to gripper fingers and replacing with synthetic point clouds through forward kinematics, 4) uniformly sampling without replacement, and 5) appending semantic labels to indicate gripper fingers (red) and the scene (blue).

### B.3 Human-in-the-Loop Data Collection

This data collection procedure is illustrated in Algorithm 1. As shown in Fig. A.6, we use a 3Dconnexion SpaceMouse as the teleoperation device. We design a specific UI (Fig. A.7) to facilitate the synchronized data collection. Here, the human operator will be asked to intervene or not. The operator answers through keyboard. If the operator does not intervene, the base policy’s next action will be deployed. If the operator decides to intervene, the SpaceMouse is then activated to teleoperate the robot. After the correction, the operator can exit the intervention mode by pressing one button on the SpaceMouse. We use this system and interface to collect 20, 100, 90, and 17 trajectories with correction for tasks *Stabilize*, *Reach and Grasp*, *Insert*, and *Screw*, respectively. We use 90% of them as training data and the remaining as held-out validation sets. We visualize the cumulative distribution function of human correction in Figure A.8.



Figure A.6: **Real workspace setup for human-in-the-loop data collection.** The human operator provides online correction through a 3Dconnexion SpaceMouse while monitoring the robot’s execution.

### B.4 Residual Policy Training

#### B.4.1 Model Architecture

The residual policy takes the same observations as the base policy (Table A.VI). Furthermore, to effectively predict residual actions, it is also conditioned on base policy’s outputs. Its action head outputs eight-dim vectors, while the first seven dimensions correspond to residual joint positions and the last dimension determines whether to negate base policy’s gripper action or not. Besides, a separate intervention head predicts whether the residual action should be applied or not (learned gated residual policy, Sec. 3.3).

---

**Algorithm 1:** Human Intervention and Online Correction Data Collection

---

**input** : Base policy  $\pi^B$ , human policy  $\pi^H$ , real-world environment  $\mathcal{E}$   
**output** : Human correction dataset  $\mathcal{D}^H$   
**initialize**:  $\mathcal{D}^H \leftarrow \emptyset$

```
 $o \leftarrow \mathcal{E}.reset()$ 
while not  $\mathcal{E}.terminated$  do
    ▷ deploy the base policy for one step
     $a^B \leftarrow a^B \sim \pi^B(o)$ 
     $o^{next} \leftarrow \mathcal{E}.deploy(a^B)$ 
    ▷ human decides intervention or not
     $1^H \leftarrow \pi^H.intervene(o, o^{next})$ 
    if  $1^H$  then
         $q^{pre} \leftarrow \mathcal{E}.robot\_state$ 
        ▷ deploy human correction
         $a^H \leftarrow a^H \sim \pi^H(o, o^{next})$ 
         $o^{next} \leftarrow \mathcal{E}.deploy(a^H)$ 
         $q^{post} \leftarrow \mathcal{E}.robot\_state$ 
        ▷ update dataset
         $\mathcal{D}^H \leftarrow \mathcal{D}^H \cup (q^{pre}, q^{post}, 1^H, o)$ 
    end
    ▷ update observation for the next step
     $o \leftarrow o^{next}$ 
end
```

---

For tasks *Stabilize* and *Insert*, we use a PointNet [86] as the point-cloud encoder. For tasks *Reach* and *Grasp* and *Screw*, we use a Perceiver [87, 88] as the point-cloud encoder. Residual policies are instantiated as feed-forward policies in all tasks. We use GMM as the action head and a simple two-way classifier as the intervention head. Model hyperparameters are summarized in Table A.IX.

Table A.IX: Model hyperparameters for residual policies.

Hyperparameter	Value	Hyperparameter	Value
PointNet		Feature Fusion	
PointNet Hidden Dim	256	MLP Hidden Dim	512
PointNet Hidden Depth	2	MLP Hidden Depth	1
PointNet Output Dim	256	MLP Activation	ReLU
PointNet Activation	GELU	GMM Action Head	
Gripper Semantic Embd Dim	128	Hidden Dim	128
Perceiver		Hidden Depth	3
Perceiver Hidden Dim	256	Num Modes	5
Perceiver Number of Heads	8	Activation	ReLU
Perceiver Number of Queries	8	Intervention Head	
Gripper Semantic Embd Dim	128	Hidden Dim	128
Base Policy Action Conditioning		Hidden Depth	3
Base Policy Gripper Action Embd Dim	64	Activation	ReLU

#### B.4.2 Training Details

To train the learned gated residual policy, we first only learn the feature encoder and the action head. We then freeze the entire model and only learn the intervention head. We opt for this two-stage training since we find that training both action and intervention heads at the same time will result in sub-optimal residual action prediction. We follow the best practice for policy training [98, 155, 164], including using learning rate warm-up and cosine annealing [89]. Training hyperparameters are listed in Table A.X.

```

(....)
system: need human intervention? (y/n)
user: n
(deploying the next action)
system: need human intervention? (y/n)
user: y
(correction through teleopeartion)
system: exiting human intervention...
(....)

```

Figure A.7: The UI for synchronized human-in-the-loop data collection.

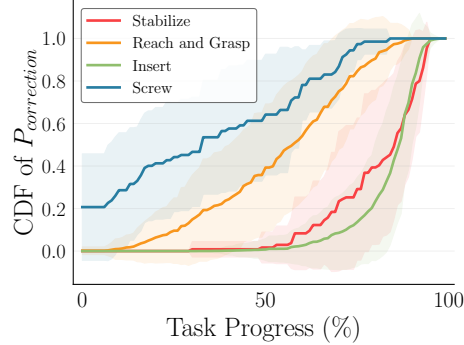


Figure A.8: **Cumulative distribution function (CDF) of human correction.** Shaded regions represent standard deviation. Human correction happens at different times across tasks. This fact necessitates TRANSIC’s learned gating mechanism.

## C Experiment Settings and Evaluation Details

In this section, we provide details about our experiment settings and evaluation protocols.

### C.1 Main Experiments (Sec. 4.2)

We evaluate all methods on four tasks for 20 trials. Each trial starts with different objects and robot poses. We make our best efforts to ensure the same initial settings when evaluating different methods. Specifically, we take pictures for these 20 different initial configurations and refer to them when resetting a new trial. See Figs. A.14, A.15, A.16, A.17 for initial configurations of tasks *Stabilize*, *Reach and Grasp*, *Insert*, and *Screw*, respectively.

### C.2 Experiments with Different Sim-to-Real Gaps (Sec. 4.3)

#### C.2.1 Experiment Setup

We elaborate on how different sim-to-real gaps are created.

**Perception Error** This is done by applying random jitter to 25% points from point clouds, which corresponds to adding noise in observation space  $\mathcal{O}$ . We test this sim-to-real gap on the task *Reach and Grasp*. As visualized in Fig. A.9, with probability  $P = 0.6$ , we apply random jitter to 25% points from the point-cloud observation. The jittering noise is sampled independently from the distribution  $\mathcal{N}(0, 0.03)$ . We clip the noise to be within the  $\pm 0.03$  range.

**Underactuated Controller** This is done by making the joint position controller less accurate, which corresponds to mismatched action space  $\mathcal{A}$ . We test this gap on the task *Insert*. We emulate

Table A.X: **Hyperparameters used in residual policy training.**

Hyperparameter	Value
Learning Rate	$10^{-4}$
Weight Decay	0
Learning Rate Warm Up Steps	1,000
Learning Rate Cosine Decay Steps	100,000
Minimal Learning Rate	$10^{-6}$
Optimizer	Adam

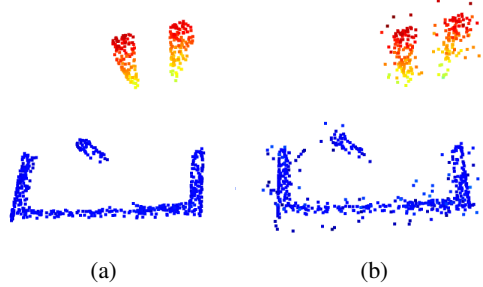


Figure A.9: **Visualization of introduced perception error.** **a)** The original point-cloud observation. **b)** The erroneous point-cloud observation with random jitter.

an underactuated controller through early stopping. Concretely, at every time a new joint position goal  $\mathbf{q}_{goal}$  is set, we record the distance to the goal in configuration space  $d_{\mathbf{q}} = \|\mathbf{q} - \mathbf{q}_{goal}\|$  and sample a factor  $\Gamma \sim \mathcal{U}(0.80, 0.95)$ . The controller will stop reaching the desired goal once it achieves  $\Gamma$  progress, i.e., stop early when  $\|\mathbf{q} - \mathbf{q}_{goal}\| \leq (1 - \Gamma)d_{\mathbf{q}}$ . Fig. A.10 visualizes the effect.

**Embodiment Mismatch** This is done by changing the robot gripper to be shorter length as demonstrated in Fig. A.11, which corresponds to discrepancy in state space  $\mathcal{S}$  and transition function  $\mathcal{T}$ . We test this gap on the task *Screw*. We notice that the 9 cm length difference incurs a significant gap.

**Dynamics Difference** This is done by changing object surfaces and increasing friction, which corresponds to different transition function  $\mathcal{T}$ . We test this gap on the task *Stabilize*. Concretely, we

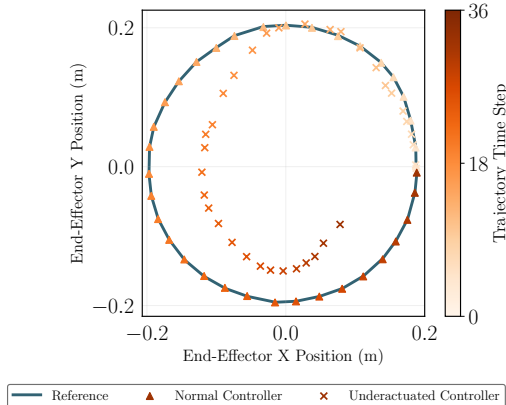


Figure A.10: **Visualization of the trajectory realized by an underactuated controller.** The plot displays the end-effector’s position in the XY plane. It shows a reference circular movement, a trajectory tracked by the normal controller, and a trajectory tracked by the underactuated controller.

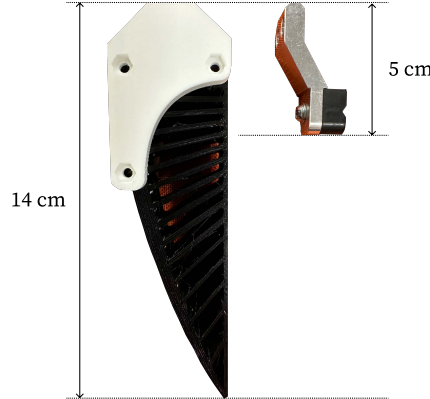


Figure A.11: **Two different gripper fingers used to create embodiment mismatch.** Policies are trained with the longer finger and tested on the shorter finger.

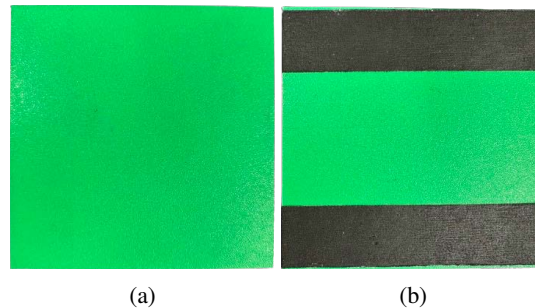


Figure A.12: **Two square tabletops used to create dynamics difference.** **a)** The original surface is smooth. **b)** We attach friction tapes to change the dynamics.

attach friction tapes to the square tabletop's surface to increase friction, hence change the dynamics (Fig. A.12).

**Object Assert Mismatch** As shown in Fig. A.13, this is done by replacing the table leg with a light bulb, which corresponds to change in emitting function  $\Omega$ . We test this gap on the task *Reach and Grasp*.

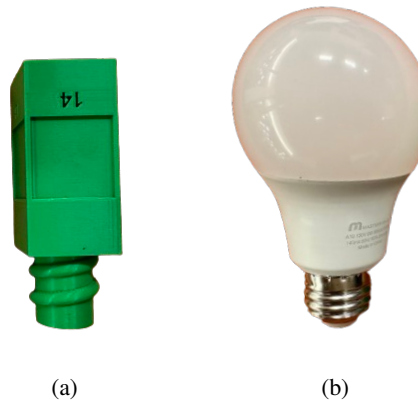


Figure A.13: **Two objects used to create asset mismatch.** **a)** Policies are trained with the table leg. **b)** We test policies with an unseen light bulb.

Table A.XI: Quantitative results for scalability with human correction dataset size on four tasks.

Method	Correction Dataset Size (%)				
	0	25	50	75	100
Stabilize					
TRANSIC IWR [67]	35%	80%	80%	100%	100%
		70%	75%	80%	65%
Reach and Grasp					
TRANSIC IWR [67]	60%	65%	80%	90%	95%
		60%	65%	40%	40%
Insert					
TRANSIC IWR [67]	5%	20%	35%	40%	45%
		5%	15%	30%	40%
Screw					
TRANSIC IWR [67]	35%	50%	65%	75%	85%
		20%	40%	40%	40%

### C.2.2 Evaluation

We conduct 20 trails with different initial configurations. Initial conditions for first four experiments are the same as main experiments (Figs. A.14, A.15, A.16, A.17). Fig. A.18 shows initial configurations for the experiment *Object Asset Mismatch*.

## C.3 Data Scalability Experiments (Sec. 4.4)

In Table A.XI, we show quantitative results for scalability with human correction dataset size on four tasks.

## C.4 Policy Robustness Experiments (Sec. 4.5)

### C.4.1 Removing Cameras

We remove two cameras and only keep three. Note that this is the same number of cameras as in FurnitureBench [90]. For tasks other than *Insert*, we keep the wrist camera, the right front camera, and the left rear camera. For the task *Insert*, we keep two front cameras and the left rear camera.

### C.4.2 Suboptimal Correction Data

We simulate suboptimal correction data by injecting noise into residual actions  $a^R$ . This noise is of large magnitude, which follows the normal distribution with zero mean and standard deviation corresponding to 5% of the largest residual action in the dataset.

## D Additional Experiment Results

### D.1 Distilling Simulation Base Policy with Diffusion Policy

We experiment with learning simulation base policies (Sec. 3.1) with the Diffusion Policy [85]. Concretely, when performing *action space distillation* to learn student policies, we replace the Gaussian Mixture Model (GMM) action head with the Diffusion Policy. Proper data augmentation (Table A.VIII) is also applied to robustify learned policies. Hyperparameters are provided in Table A.XII.

**Table A.XII: Diffusion Policy hyperparameters.**

Hyperparameter	Value	Hyperparameter	Value
Architecture	UNet	$T_o$	2
UNet Hidden Dims	[64, 128]	$T_a$	8
UNet Kernel Size	5	$T_p$	16
UNet GroupNorm Num Groups	8	Num Denoising Steps (Train)	100
Diffusion Step Einbd Dim	128	Num Denoising Steps (Eval)	16

The comparison between GMMs on the real robot is shown in Table. A.XIII. We highlight two findings. First, the significant domain difference between simulation and reality generally exists regardless of different policy modeling methods. Second, since the Diffusion Policy plans and executes a future trajectory, it is more vulnerable to simulation-to-reality gaps due to planning inaccuracy and the consequent compounding error. Only executing the first action from the planned trajectory and re-planning at every step may help, but the inference latency renders the real-time execution infeasible.

**Table A.XIII: The real-robot performance difference between GMM and Diffusion Policy.** The policy error caused by simulation-to-reality gaps will be amplified by the Diffusion Policy because it plans and executes a future trajectory.

	Average	Stablize	Reach and Grasp	Insert	Screw
GMM	33.7%	35%	60%	5%	35%
Diffusion Policy	22.5%	35%	50%	5%	0%

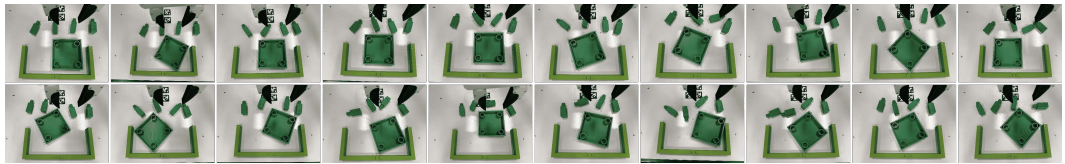


Figure A.14: Initial settings for evaluating the task *Stabilize*.

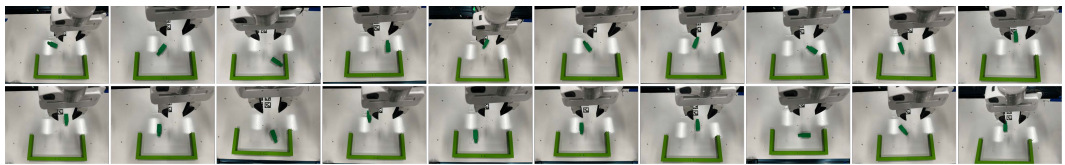


Figure A.15: Initial settings for evaluating the task *Reach and Grasp*.

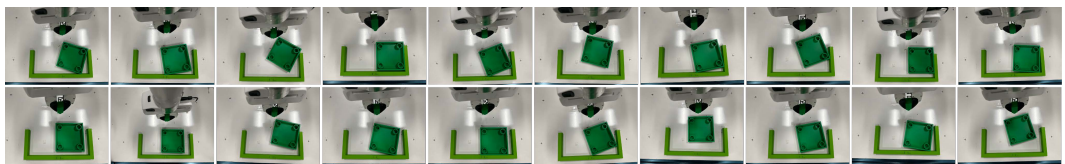


Figure A.16: Initial settings for evaluating the task *Insert*.

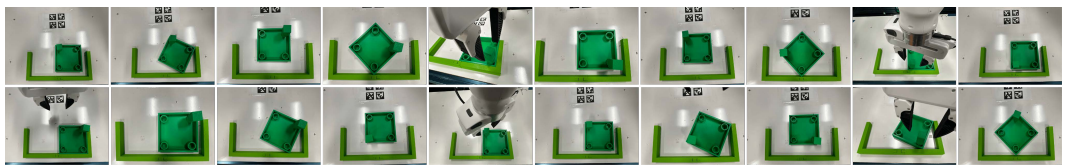


Figure A.17: Initial settings for evaluating the task *Screw*.

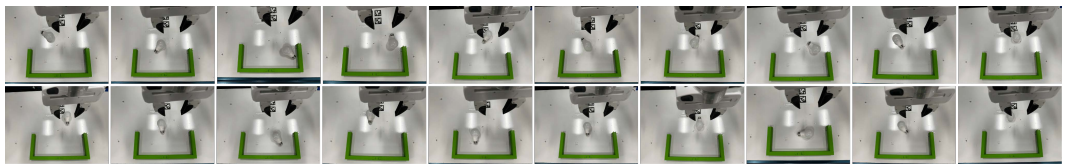


Figure A.18: Initial settings for the experiment *Object Asset Mismatch*.